



HAL
open science

Past Amazon Basin fluvial systems, insight into the Cenozoic sequences using seismic geomorphology (Marañón Basin, Peru)

Gérôme Calvès, Ysabel Calderon, Vincent Roso, Cédric Bonnel, Martin
Roddaz, Stéphane Brusset, Patrice Baby, Peter Clift

► To cite this version:

Gérôme Calvès, Ysabel Calderon, Vincent Roso, Cédric Bonnel, Martin Roddaz, et al.. Past Amazon Basin fluvial systems, insight into the Cenozoic sequences using seismic geomorphology (Marañón Basin, Peru). *Journal of South American Earth Sciences*, 2019, 90, pp.440-452. 10.1016/j.jsames.2018.12.019 . hal-02375767

HAL Id: hal-02375767

<https://hal.science/hal-02375767>

Submitted on 21 Oct 2021

HAL is a multi-disciplinary open access archive for the deposit and dissemination of scientific research documents, whether they are published or not. The documents may come from teaching and research institutions in France or abroad, or from public or private research centers.

L'archive ouverte pluridisciplinaire **HAL**, est destinée au dépôt et à la diffusion de documents scientifiques de niveau recherche, publiés ou non, émanant des établissements d'enseignement et de recherche français ou étrangers, des laboratoires publics ou privés.



Distributed under a Creative Commons Attribution - NonCommercial 4.0 International License

1 **Past Amazon Basin fluvial systems, insight into the Cenozoic sequences using**
2 **seismic geomorphology (Marañón Basin, Peru).**

3 Authors: Gérôme Calvès^{1,*}, Ysabel Calderon^{1,2}; Vincent Roso³; Cédric Bonnel³; Martin Roddaz^{1,4}; Stéphane
4 Brusset¹, Patrice Baby⁴, Peter D. Clift⁵

5 1. Université Toulouse 3, GET-OMP, 14 Avenue Edouard Belin, 31400, Toulouse, France. *Corresponding author:
6 gerome.calves@get.omp.eu

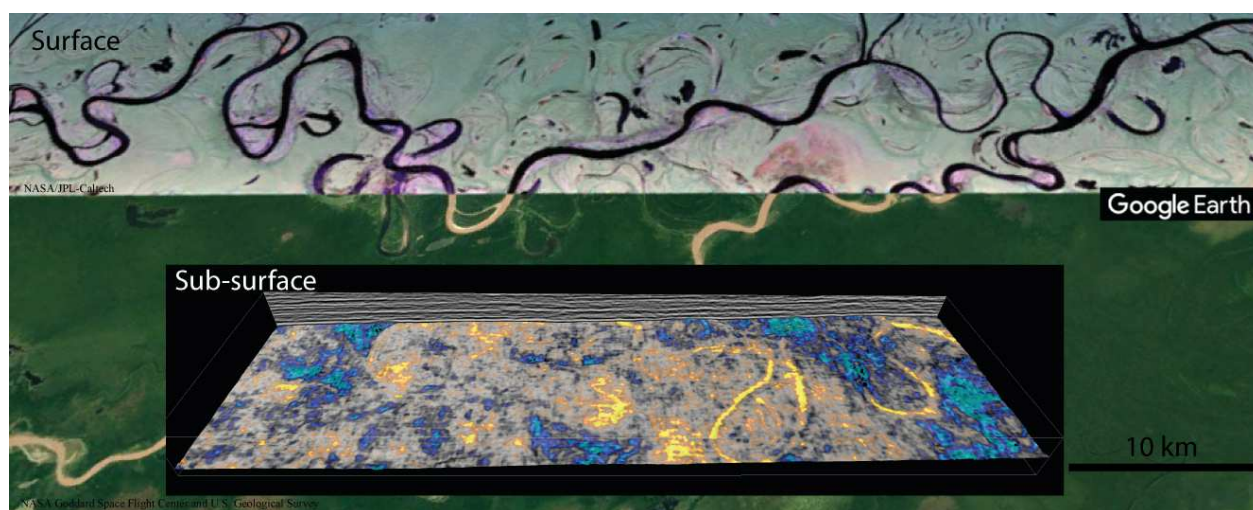
7 2. PeruPetro, Lima, Peru

8 3. LFC-R, Université de Pau et des Pays de l'Adour, Avenue de l'Université, 64013, Pau, France.

9 4. IRD, GET-OMP, 14 Avenue Edouard Belin, 31400, Toulouse, France

10 5. Louisiana State University (LSU), Baton Rouge, Louisiana 70803, USA

11 **Graphical Abstract:**



13 **Highlights:**

14 - 3D seismic characterization of buried fluvial systems in the Marañón Basin of Peru

15 - Evidence of ancient “big rivers” scaled to the modern Amazon Basin fluvial system

16 - Implications for evolution of sediment load and erosion history of the Andes

17

18 **ABSTRACT** (253 words)

19 This study of the seismic geomorphology of riverine deposits describes and discusses the spatial
20 resolution at which we can detect fluvial features and how the subsequently collected data can
21 help with our understanding of ancient fluvial reservoirs. For this assessment we use three
22 dimensional seismic reflection data, borehole data from ancient deposits in the Marañón foredeep
23 basin of Peru, as well as digital elevation and satellite imagery data from the present day fluvial
24 systems of the Amazonian Basin in the same area of Peru. Based on seismic stratigraphic
25 principles on amplitude display we test parameters to highlight the details of the internal structure
26 of horizons interpreted on continuous wavelets. Seismic attributes such as amplitude, phase,
27 sweetness and spectral decomposition techniques have been successfully applied to make a
28 framework of seismic stratigraphic surfaces that highlight the internal architecture and
29 morphologic details of the studied intervals. This work confirms the presence of a Cenozoic
30 fluvial system in Peru with straight, meandering and anastomosing channels. The observed
31 fluvial features are associated with narrow to medium sized channels (10~700 m). Evolution of
32 parameters such as sinuosity allows the variation of load in the identified channel features to be
33 constrained. Cenozoic Marañón Basin rivers/streams size and shape are comparable to those
34 observed in the present-day fluvial Amazon Basin. The fluvial dynamics in the study area are
35 identified to be at least present since the deposition of the Pozo-Chambira Formation (Eocene-
36 Oligocene) in the Marañón Basin.

37 **Keywords:** Seismic geomorphology, fluvial systems, meanders, channels sinuosity, Amazon
38 Basin, Cenozoic.

39

40 **1. INTRODUCTION**

41 Paleogeomorphology and drainage organization of fluvial settings has long been of great interest
42 for resource/energy, life habitat, earth cycle research (e.g. Martin, 1966; Southwood, 1977;
43 Fisher et al., 2007) due to the architectural complexity of these types of natural reservoirs and
44 environments. Observations from present-day earth surface fluvial systems are commonly used to
45 inform subsurface interpretation of fluvial-system seismic geomorphology (Posamentier, 2003).
46 Limited publications document ancient river deposits in the subsurface, most of which were
47 deposited in marine-to-fluvial or lacustrine-to-fluvial transition zone settings (e.g.: Weber, 1992;
48 Hardage and Remington, 1999; Posamentier, 2001; Miall, 2002; Sarzalejo and Hart, 2006;
49 Ethridge and Schumm, 2007; Wood 2007; Zeng , 2007; Maynard et al., 2010; Reijenstein et al.,
50 2011; Hubbard et al., 2011; Wang et al., 2012; Qi'an et al., 2015; Zhuo et al., 2015; El-Mowafy
51 and Marfurt, 2016; Alqahtani et al., 2017).

52 Despite this effort to address some of the most studied objects in the rock record, rivers and their
53 deposits continue to be problematic to earth scientists (Miall, 2014). “Big rivers” are the main
54 arteries that deliver the water and sediment from both orogenic and non-orogenic areas of
55 continents to the world’s oceans (Potter, 1978; Miall, 2006; Ashworth and Lewin, 2012; Lewin
56 and Ashworth, 2014). Reconstructing big rivers from ancient deposits is especially challenging
57 due to difficulties in measuring/identifying (and scaling) the architectural elements composing
58 past big rivers. Such deposits are often beyond the scale of conventional outcrops. However, 3D
59 seismic offers the spatial extent to capture the full scale of these elements (Bridge and Tye, 2000)
60 and enables characterization of many ancient rivers whose scale may rival the ‘big rivers’ of the
61 modern world, such as the Amazon River.

62 The Amazon River (Figure 1A) ranks number one in terms of global mass transfer from the
63 continents to the oceans (Figure 1B). Indeed, the Amazon River supplies about 20% of the water
64 (Callède et al., 2004), ~10% of the dissolved load (Gaillardet et al., 1997) and ~3% of the
65 suspended load (Milliman and Syvitski, 1992) to the world's oceans. These numbers for transport
66 are only surpassed by the sediment yield in the rivers of south and south-east Asia such as the
67 Huanghe or the Ganges-Brahmaputra (Figure 1B). The present day Amazon Basin is covered by
68 dense tropical vegetation partly protected by nature reserves and is drained by major rivers
69 (Figure 1C). The detailed architecture of the river and its floodplain can be revealed by modern
70 airborne data acquisition, such as Uninhabited Aerial Vehicle Synthetic Aperture Radar
71 (UAVSAR) (Figure 1C). Satellite imagery allows clear discrimination of the two primary
72 elements of this system: the river loaded by suspended fine sediments and the lateral floodplain
73 covered by vegetation.

74 Recent studies of the outer continental shelf and uppermost Amazon deep-sea fan sediments
75 suggest that the Amazon River initiated as a transcontinental river between 11.8 and 8.7 Ma
76 (Figueiredo et al., 2009; Gorini et al., 2014; Hoorn et al., 2017; van Soelen et al., 2017), and
77 reached its present shape and size during the late Pliocene (Figueiredo et al., 2009). Before the
78 Amazon River transected South America the Middle Miocene environment of the study area was
79 characterized by a long-lived mega-wetland, the Pebas system (Wesselingh et al., 2009; Hoorn et
80 al., 2010). Before the Neogene, the drainage of the Amazon River is postulated to have been to
81 the North with a probable river mouth in the Maracaibo Lake (Roddaz et al., 2010. Hurtado et al.,
82 2018).

83 The stratigraphy of the Marañón Basin is characterized by two sequences related to the pre-
84 Andean series that consists of Paleozoic–Mesozoic deposits and the Andean series that

85 corresponds to Cenozoic marine to continental foreland successions (e.g. Hermoza et al., 2005;
86 Roddaz et al., 2010; Baby et al., 2013; Calvès et al., 2018; Hurtado et al., 2018). Stratigraphic
87 analysis of the continental and fluvial record of the foreland succession (e.g.: Latrubesse et al.,
88 2010) has improved over the past decades with documentation of marine incursion in a globally
89 continental sequence (Westaway, 2006; Wesselingh et al., 2009; Hoorn et al., 2010; Roddaz et
90 al., 2010; Rebata et al., 2016; Jallamillo et al., 2017). In contrast, the structural control on
91 sedimentation and river location in this context has received limited attention (Dumont et al.,
92 1991; Räsänen et al., 1992; Roddaz et al., 2010; Gross et al., 2011; Kröhling, 2017).

93 The objective of our study is to document the detailed structure of the paleo-fluvial Amazonian
94 system using 3D seismic geomorphology techniques and compare these images to the present day
95 surface drainage geometry of the Amazon Basin in order to discuss the evolution and the
96 preservation of large-scale river deposits in continental drainage areas.

97 **2. MATERIALS AND METHODS**

98 To document the evolution of the present day and paleo-landscape of the Marañón Basin in the
99 Amazon drainage, we have used two data sets. The main data set is 3D multi-channel, post-stack,
100 time-migrated reflection seismic. These data have been acquired over the past decades over oil
101 and gas fields in the Marañón Basin in Peru (Figure 2). The seismic data displayed in this study
102 are zero phase, and follow the Society of Exploration Geophysicist normal polarity, i.e. black
103 peaks indicating an increase in acoustic impedance. The areal extent of the 3D cube is from 90
104 km² to 190 km². The 3D grid is subdivided into in-line and cross-line directions, spaced at 30 m.
105 The sampling rate is 4 ms two-way travel time (TWT). In the shallow subsurface the frequency
106 range is 10-70 Hz, with a dominant frequency in the 20-50 Hz range.

107 Borehole information has been used to constrain the stratigraphy over this area in conjunction
108 with standard seismic stratigraphic principles. The seismic data have been interpreted using
109 various techniques (horizon picking, stratal slicing) and various seismic attributes (Taner and
110 Sheriff, 1977; Taner et al., 1979; Taner, 2003) such as amplitude, phase, sweetness (Hart, 2008) or
111 thin-bed indicators have been extracted and used to enhance interpretation (Figure 3). To screen
112 the data and allow the reader to scroll through the volume, we have extracted seismic amplitude
113 on stratal horizons, and compiled them to produce an animated movie (supplementary data;
114 movie: Hor_slice_Amp.mpg and metadata). A seismic facies chart has been established based on
115 the geometries and acoustic properties observed and quantified on vertical sections and horizontal
116 displays within the 3D volumes. The seismic facies (SF) identified are summarized in Figure 4.

117 We interpret the morphologic elements found in the 3D data and compare these to morphologies
118 observed in present day river systems (Posamentier, 2000). To accomplish the later, we utilized
119 our second primary data set, satellite images and digital elevation models (DEMs) from the
120 present day surface of the Amazonian Basin. We have used public satellite images and airborne
121 radar (<https://uavsar.jpl.nasa.gov>), as well as digital elevation models from the NASA Shuttle
122 Radar Topography Mission (SRTM) (<https://www2.jpl.nasa.gov/srtm/>).

123 Geomorphological features such as channels (Figure 5) have been quantified following the
124 scheme developed by previous workers on quantitative seismic geomorphology of fluvial
125 features (e.g. Miall 2002; Wood, 2007; Ethridge and Schumm, 2007). Measurements are
126 summarized in Table 1. Parameters of alluvial channels and classification are sourced from
127 Schumm (1985). Paleocurrent flow direction of the fluvial features (trunk rivers, channel, and
128 meander) has been determined following the methods of Miall (2000).

129 **3. RESULTS**

130 **3.1. Seismic stratigraphy of the Marañón Basin**

131 The Marañón Basin is a foredeep depozone of the Northern Amazonian foreland basin located
132 between the Andes to the West and the Brazilian and Guyanan shields on its eastern flank (Figure
133 2). Part of its eastern side is constituted by the Iquitos forebulge (Roddaz et al., 2005) (Figure
134 2A). We have focused our study on the Cenozoic infill of this basin (Figure 2B), which
135 comprises a thick pile (>3500 m) of clastic sedimentary rocks sourced from the Andes and the
136 South American Cratons. Above the Casablanca-Yahuarango Formation (Cretaceous to lower
137 Paleogene, Figure 2C), the overlying Pozo Shale and Pozo Sandstone (Hermoza et al., 2005)
138 marks the initiation of an overall aggrading fluvial sequence (Chambira, Pebas, Marañón and
139 Corrientes Formations). The seismic images associated to this sequence are characterized by
140 regional >100 km continuous to discontinuous reflections (Figure 2B). At the field scale (less
141 than 10 km), these stratal amplitudes show slight vertical discontinuities (<10–20 ms TWT).
142 These are marked by bright amplitude and high sweetness compared to background values
143 (Figures 3A and 3B). These discontinuous reflections are marked on their edge by phase changes
144 (Figure 3C) and tuning effects marked by the thin-bed detector attribute (Figure 3D).

145 Below we describe the observations made based on calibrated 3D seismic reflection images. We
146 further interpret these observations in the context of the morphologies that characterize the
147 sedimentary section and summarize its evolution during the Cenozoic.

148 **3.2. Seismic geomorphology of the Paleo-Amazon drainage system**

149 The main seismic facies observed in the studied interval are summarized in Figure 4. Features
150 observed in vertical seismic section are associated with their plan view observed on horizon

151 amplitude extraction. Discrimination of facies in this fluvial environment cannot be solved only
152 on 2D vertical seismic display. The conformable and parallel seismic reflection makes the plan
153 view and amplitude information essential in recognizing sedimentary features interpreted as
154 channel and streams. Eight SFs have been identified (Figure 4). Seismic facies SF1 to SF5 are
155 interpreted to represent fluvial meandering features, each with various degrees of sinuosity and
156 channel widths that flowed without cross-cutting relationship, whereas seismic facies SF6 is
157 interpreted to reflect deposits from similar types of channels but exhibiting crosscutting
158 relationships. Seismic facies SF7 is interpreted to represent an anastomosing fluvial network.
159 Seismic facies SF1-SF7 occur within a background facies of channel-free material, that is herein
160 interpreted as floodplain overbank sediment (SF8). The peak frequency of these seismic facies
161 ranges from 15 to 45 Hz. The velocity range of the section based on sonic measurement is ~1850
162 m/s in the shallower section and up to 3800 m/s in the deepest part of the investigated section
163 (over 2.5 sTWT). These velocity values enable bed thickness to be estimated (1/4 wavelength;
164 e.g. Sheriff, 1992) at ~40 m for the higher frequency in the upper section and ~250 m for the
165 lower frequency in lower section. Channels and related parameters have been quantified in plan
166 view following the parameters defined in Figure 5. Channel-widths range from 40 to >650 m
167 (Figure 4). The larger channels show sedimentological features interpreted as channel bars,
168 meander cut-offs and lateral migration of meanders of various sinuosities. The channels can be
169 ranked in three categories based upon their width, following the classification of Gibling (2006).
170 This is as follows: narrow to medium 10s of meters width for individual channels, >100 m wide
171 medium scale composite channels, and >1000 m – wide fluvial systems. Seismic geomorphologic
172 analysis of eight sequential decomposition RGB blended stratal horizon slices provides a
173 temporal history from youngest to oldest stratigraphic levels (Figure 3A; Horizons 8 through 1)
174 and as shown in Figure 6. The seismic facies are interpreted with three main types of fine grained

175 sediment (mostly shale and silt) associated with splay and other flood plains sediments, as well as
176 two coarse grained lithologies (mostly sand to gravels) associated with channel fills and channel
177 belts.

178 The oldest horizon within the Marañón Formation, Horizon 8 (pink, Figures 3A and 6A),
179 displays a main channel running in a WNW-ESE trend that is connected to narrow, sparsely-
180 spaced linear to low sinuosity streams. The underlying horizon, Horizon 7, is interpreted to be the
181 Pebas Formation and shows a denser network of parallel medium-to-wide channels associated
182 with rare meandering narrow channels (red, Figure 6B). Horizon 6 shows the transition from
183 Pebas to Chambira Formations and is marked by the interconnection of medium-to-wide channels
184 with N-S to W-E orientations (orange, Figure 6C). Horizon 5, the top of the Chambira Formation
185 (yellow, Figure 6D) shows well developed densely developed interval of high sinuosity, medium
186 width meandering channels. The upper Chambira Formation, Horizon 4 (light green, Figure 6E)
187 shows a greater frequency of wide channels without any characteristic orientation. The channels
188 in this interval show intricate meandering architecture. The transition from upper to lower
189 Chambira Formation at Horizon 3 shows sinuous channels with a potentially anastomosing
190 organization (deep green, Figure 6F). The next underlying interval shown on Horizon 2 is
191 interpreted as the lower Chambira Formation, and shows isolated NNE-SSW oriented, wide
192 meandering belts with high sinuosity meander scars (light blue, Figure 6G). Finally, the oldest
193 Horizon 1, is representative of the Pozo Formation that is characterized by a set of sinuous
194 parallel W-E channels with narrow to medium in width (marine blue, Figure 6H).

195 **3.3. Quantification of channels and fluvial features properties**

196 Quantification of the channel width ($n = 420$) from the studied seismic horizons interpreted from
197 the Pozo to the Marañón Formations allows a frequency analysis to be conducted and illustrated

198 by the histogram (Figure 7). The median channel width is 121 m ($\sigma = 107$ m). Minimum channel
199 width is 29 m and the maximum value is 641 m (Figure 7A). Based on fluvial channel
200 classifications (Gibling, 2006) 36% of the measured population is classified as being narrow
201 channel. The others are associated to the medium channel group, that have at least of 100 m
202 width. No individual channel features measured in the study area are wider than 641 m. The
203 median channel belt width ($n = 83$) is 3598 m ($\sigma = 1295$ m), with a minimum measured width of
204 994 m and a maximum of 7187 m (Figure 7B).

205 The sinuosity of meandering channels has been quantified ($n = 84$; Figures 5 and 8) on plan view.
206 The median sinuosity is 1.4 ($\sigma = 0.47$) with a minimum value of 1 and a maximum value of 2.9.
207 About 40% of the measured channels have a sinuosity lower than 1.4. Based on the classification
208 scheme of Schumm (1985) for channel sinuosity and load, the measured channels can be divided
209 as follows: with bedload (29.8%) and a sinuosity lower than 1.3, related to a mixed load (53.6%)
210 and a sinuosity higher than 1.3 but and lower than 2, and to suspended load (16.7%) with a
211 sinuosity higher than 2 (Figure 8).

212

213 **3.4. Temporal evolution and dynamics of Paleo-Amazon drainage system**

214 The Cenozoic evolution of the fluvial architecture of the basin fill is summarized through three
215 parameters (channel width, channel belt width and sinuosity) and measurements of paleocurrent
216 directions (Figure 9). Channel width evolves up-section with apparent increasing size from the
217 Pozo Formation (horizon H1, Figure 9A) to the Chambira Formation (Horizon H2, Figure 9A).
218 Within the Chambira Formation, the upper member shows an increase in channel width with
219 peaks up to 400 m between Horizons H3 and H4, and up to >600 m width between horizons H4
220 and H6 (Figure 9A). The upper units of the Chambira Formation show a decrease in channel

221 width that increase again slightly in the upper part of the section, between the Pebas and Marañón
222 Formations (horizons H6 to H8; Figure 9A). The channel belt width increases in association with
223 the type of facies and fluvial patterns, especially with the occurrence of high sinuosity streams
224 (Figures 9B and C). The channel belt width is narrow (~2 km) in the Pozo Formation (H1) while
225 it increase during the emplacement of the Chambira Formation (up to 7.2 km). Then, it decreases
226 in the upper part of the Chambira Formation (horizons H5-H6) and in the Pebas Formation (H7),
227 and finally increase slightly in the Marañón Formation (above H8, Figure 9B). This evolution is
228 highlighted by the sinuosity parameter (Figure 9C). In the same area, the observed modern
229 sinuosity is around 2 where there is the transition from mixed to bed load types (Schumm, 1985).
230 The Pozo Formation fluvial deposits are characterized by sinuosity over 2 and is associated with
231 suspended load transport (horizon H1; Figure 9C). The sinuosity of the Chambira Formation
232 shows a lower member (horizons H2 to H4; Figure 9C) with values associated with low to
233 moderate values (bed load and mixed load) and occasional high values (suspended load). The
234 Upper Member of the Chambira Formation (horizons H5 to H6; Figure 9C) shows low values of
235 sinuosity (mainly bed load). The Pebas and Marañón Formations (horizons H7 to H8; Figure 9C)
236 show mainly low values with some rare high values of sinuosity. The evolution of paleocurrents
237 follows a two steps evolution with NE and SE flowing streams during sedimentation of the Pozo
238 Formation. A wide, south-directed flow was observed during deposition of the Chambira
239 Formation, while a more SE-ward direction of flow was noted for the Pebas and Marañón
240 Formations (Figure 9D). This sequence of aggrading stacked streams and rivers contains three
241 main fluvial features, including: straight, meandering and anastomosing channels (Figure 4 and
242 supplementary data; movie: Hor_slice_Amp.mpg and metadata).

243 **3.5. Present day proximal Amazon drainage and rivers**

244 The present day surface of the Amazon Basin is characterized by a W to E oriented drainage
245 (Figure 1A) with rivers that are both controlled by and incising into topographical structures
246 (Figure 10A) related to the recent evolution of the South American Plate and the Andean
247 mountain range (e.g.: Räsänen et al., 1987, 1990, 1992; Roddaz et al., 2005; Shephard et al.,
248 2010; Latrubesse, 2015; Stokes et al., 2018). The Marañón Basin sits at the confluence of two
249 main river networks, one originating from the Napo-Pastaza Fan to the northwest (Figure 10A;
250 Bernal, et al., 2011) and a second from the Fitzcarrald Arch to the southwest (Espurt et al., 2007).
251 These two drainages combine at the town of Iquitos to form the Rio Solimões that run to the
252 Amazon River mouth and from there into the Atlantic Ocean. An SRTM digital elevation model
253 has been extracted to document the shape and size of the rivers and drainage from the Andes to
254 Iquitos (Figure 10B to 10E). The NW-SE present river located above the seismic cube is the Rio
255 Pataza (Figure 6 and supplementary data movie). We have seen that since the Cenozoic the river
256 network and types evolved in two major steps recorded by the Pozo, Chambira, Pebas and
257 Marañón Formations. Downstream the rivers are able to incise the edge of the older watershed,
258 related with the recent rise of the Iquitos Arch along a NW-SE axis (Figure 10C). An incision is
259 presently filled by highly sinuous meanders and streams that are controlled by kilometer wide
260 lows (Figure 10C). Laterally the Pastaza-Corrientes transition band (Figure 10A) with its low
261 land and flood plains shows rivers that are isolated with more linear streams and lower sinuosity
262 (Figure 10D). Finally, after the connection of the Rio Tigre, Marañón and Ucayali, a wide to very
263 large river flows to the NE with large point bar and cut off (Figure 10E). All these present day
264 settings represent the large diversity of rivers and streams along this proximal part of the Amazon
265 Basin.

266 **4. DISCUSSION**

267 **4.1. Comparing present day and past morphologies of rivers using different images sources**

268 We have documented the seismic geomorphology of the sedimentary infill of part of the Marañón
269 Basin and the present day fluvial network of the western Amazon Basin. The areal cover and
270 vertical penetration of the subsurface data allows channels associated to a paleo-river network to
271 be recognized. Characterization of the vertical resolution of a channel in subsurface imaging is a
272 difficult task, whereas the lateral extend is easier to achieve. In contrast, measurements of lateral
273 extent based on downhole wireline logs is challenging (Bridge and Tye, 2000) but thickness is
274 easy to quantify (e.g.; Gibling, 2006). Here we discuss the sizes, shape recognition and potential
275 risk when using analogues and various sources of data displayed in plan view analysis, i.e. the
276 comparison of relative resolution (Figure 11). From a high resolution UAVSAR image, a Landsat
277 image or a stratal seismic horizon we can try to understand the predictive nature of the
278 observations. From a giant meander in the Rio Ucayali, a reference 5x5 km box allows a river
279 and its internal structures such as meanders, bars, oxbow lakes or a portion of them to be framed
280 regardless of where the box is located (Figure 11A). Using a set of Landsat images (Figure 11B),
281 we can characterize the shape of various rivers even for the widest meanders, oxbow lakes and
282 bars. However, the lateral continuity of the channel laterally cannot be described. In contrast, the
283 3D images of the channels derived from the seismic reflection data allow a mixed perspective
284 with a lower resolution (Figure 11C). A 5x5 km box applied to a given 3D stratal horizon allows
285 the definition of the channel and its content, especially when using spectral decomposition and
286 color blend display (Partyka et al., 1999). Targeting channels and their net infill is the goal of
287 natural resources exploration if such work is to define good quality reservoirs. Comparison of the
288 ancient geologic reservoir and its present day analogues can help to assist with reservoir
289 properties prediction (Alexander, 1993; Clift et al., 2018). The fluvial sedimentary environment

290 is a challenge because the shape of a river can be associated with various locations on the
291 erosional-depositional profile and upstream controls (Schumm, 2005).

292 **4.2. Persistent fluvial landscape**

293 The fluvial features described above characterize most of the Cenozoic infill of the Marañón
294 Basin and the present day surface of the Amazon Basin. Our study outlines the preservation of
295 fluvial geomorphic elements in the rock record, as observed in modern sedimentary basins
296 (Weissman et al., 2015). The difficulty in establishing long-term quantified rates of
297 sedimentation and related supply from mountain ranges could be solved using the fluvial features
298 observed in the subsurface. The morphology of the present day Amazon Basin and its
299 meandering rivers and floodplain are driven by the sediment supply (Constantine et al., 2014).
300 Thus, investigation of calibrated fluvial features could allow the paleo-sediment supply of the
301 Cenozoic Andes to the Amazon Basin to be quantified.

302 The role of deep solid-earth structure on the vertical movements of the Earth's surface and the
303 processes related to drainage/fluvial dynamics at continental scale has been investigated (e.g.,
304 Flament et al., 2015; Rodríguez Tribaldos et al., 2017). Limitation of the models mean that the
305 earlier history of the Amazon Basin cannot be solved in this way. The Late Eocene to Early
306 Oligocene times are predicted to represent periods of low incision rates over the entire Amazon
307 catchment (Rodríguez Tribaldos et al., 2017). Incision rates increased in the Early Miocene in
308 those areas west of the Guyana and Brazilian Cratons. The incision rate near the Cordillera only
309 increased at 11 Ma. Our observations of the early dynamics of incision and deposition of fluvial
310 system in the proximal part of the Amazon Basin near the Cordillera are in agreement with this

311 timing of uplift. Fluvial systems of continental drainage have existed since the transition from the
312 Pozo to the Chambira Formations, i.e., at least since the Oligocene.

313

314 **5. CONCLUSIONS**

315 Modern techniques of seismic imaging and geomorphology have allowed the sedimentological
316 evolution of the Marañón Basin in Peru to be reconstructed. We document the fluvial history of
317 the Amazon Basin at the scale of the Cenozoic for the first time. This sequence of an
318 aggradational stack of streams and rivers contains three main fluvial features, including straight,
319 meandering and anastomosing channels. The size and shape of the channels observed are
320 comparable with present day observations from DEMs or satellite images of Amazon Basin
321 drainage and its river network. This study represents a first step toward a methodology for
322 regional exploration of the fluvial record through the use of modern seismic geomorphology
323 techniques in the Amazon Basin. Yet far from answering all the points raised by other studies of
324 fluvial geomorphology, further detailed mapping of the Cenozoic sedimentary basins of the
325 Amazon Basin is needed (e.g. Solimões, Amazonas). These work must stretch from the source to
326 the sink if it is to depict the sediment routing systems (Allen, 2017), from the foothills of the
327 Andes Mountains to the Amazon mouth and its slope margin deep-water fan. Specific aspects
328 that need to be developed and tested included: (1) integration of borehole resistivity imagery to
329 constrain paleoflow of stream and rivers, (2) quantitative geomorphology and stream flow
330 orientation, (3) combining tracer techniques of sediments to define the sources of sediments.
331 Update of the paleogeographic map for this specific period of geological time will allow better
332 constraints on the evolution of the South American plate that is relatively inaccessible to field

333 study compared to other continents. Acquisition of vertical ‘transitional’ subsurface data ranging
 334 from the surface to the youngest resolved seismic reflection image in subsurface could allow a
 335 full and continuous analysis of the evolution of this giant sedimentary basin.

336 **ACKNOWLEDGEMENTS**

337 GC would like to thank PeruPetro for allowing this work being published. Financial support from
 338 Institut-Carnot IsiFor (Agence National de la Recherche) is appreciated. Thanks to IHS-
 339 Kingdom, dGB Earth Sciences OpendTect and GeoTeric, for their academic software donations
 340 and support. Palaeocurrent diagram were produced using freeware Rose 2.1.0 (Todd Thompson
 341 Software). Many thanks to A. Hartley (University of Aberdeen) and S. Leleu (ENSEGID -
 342 IPBordeaux) for earlier discussion and perspectives on fluvial sedimentary systems. Thanks to C.
 343 Série (ConocoPhillips) and C. Kirkham (University of Oxford) for help during the manuscript
 344 revision. An earlier reviewed version of this work has benefited from valuables review performed
 345 by L. Wood (Colorado School of Mines), Y. Sun (Chevron), and J. Bhattacharya (University of
 346 Houston). Tiago Alves (Cardiff University), an anonymous reviewer, the managing editor Kerry
 347 McCarney-Castle and the regional editor Victor Ramos, are thanked for their support and
 348 constructive comments.

349 **TABLES**

350 Table 1: Channels morphometry from Marañón Basin Cenozoic infill, Peru

Horizon number	Seismic Stratigraphy	Formation name	Depth		Channel Width				Channel length on one wavelength (La)	Meander wavelength
			min	max						
			s (TWT)		(m)				(m)	(m)

1		Maranon	0,479	0,661	200	220	260	140	120	9832	464
2			0,499	0,681	130	141	87	140	145	6058	495
3			0,519	0,701	166	147	162	146	167	9328	360
4			0,557	0,727	113	170	79	120	105	7719	540
5	H8		0,587	0,757	128	162	205	154	213	7760	687
6			0,617	0,787	119	125	116	154	190	5611	320
7			0,659	0,828	188	180	102	148	134	5189	246
8			0,684	0,845	106	160	125	122	125	2620	221
9			0,7	0,864	97	120	113	80	97	7842	706
10			0,72	0,884	144	68	58	74	158	4825	453
11			0,747	0,902	242	305	88	98	65	8355	792
12			0,757	0,9112	123	101	155	74	90	5007	363
13			0,767	0,922	131	94	76	117	44	4279	340
14	H7	Pebas	0,791	0,947	213	118	85	115	51	4306	305
15			0,824	0,984	101	121	112	71	146	6987	627
16			0,843	0,992	73	95	123	46	67	3951	380
17			0,868	1,019	102	68	70	130	68	7747	535
18			0,892	1,048	70	64	84	89	149	9423	426
19			0,902	1,067	76	82	60	91	81	3283	281
20			0,912	1,077	100	117	124	109	156	6696	556
21			0,922	1,087	104	50	42	59	54	3901	312
22			0,94	1,082	65	75	104	88	42	5998	410
23	H6		0,95	1,092	97	96	118	73	159	10205	922
24			0,975	1,117	134	95	127	68	88	5050	408
25			1	1,142	143	71	94	62	46	3227	268
26			1,004	1,17	109	55	74	29	55	1645	147
27			1,024	1,19	106	166	88	96	180	4693	318
28			1,064	1,219	294	223	259	157	293	6877	601
29			1,084	1,239	99	131	86	50	171	3439	305
30			1,104	1,259	421	494	350	343	403	15083	1458
31			1,124	1,279	358	288	249	178	282	6435	426
32			1,144	1,299	527	615	503	301	615	8369	806
33			1,186	1,327	472	118	159	308	74	7783	400
34			1,201	1,355	450	222	401	617	439	11117	1045
35			1,221	1,378	97	329	138	197	162	14302	1194
36	H5		1,241	1,395	200	560	312	169	286	6604	347
37			1,261	1,415	425	149	282	223	235	4427	325
38			1,296	1,442	293	136	302	204	121	6375	455
39			1,316	1,462	215	79	79	260	161	5346	220
40			1,348	1,495	127	94	97	103	145	9842	642
41			1,377	1,519	627	641	594	550	221	20960	1837
42			1,406	1,543	168	357	262	372	437	13962	1203

43			1,424	1,566	142	236	246	279	198	7017	610
44			1,442	1,589	81	98	71	90	64	8471	455
45	H4		1,46	1,613	250	169	55	74	38	5787	459
46			1,47	1,623	166	168	262	70	155	5272	410
47			1,498	1,632	233	333	444	353	404	12693	701
48			1,532	1,661	169	189	188	222	232	9495	466
49			1,549	1,677	113	117	101	50	110	10349	584
50			1,566	1,693	189	249	171	140	306	8724	458
51			1,583	1,712	168	109	87	136	137	6086	351
52	H3		1,6	1,73	134	183	95	123	91	5915	394
53			1,61	1,74	98	156	127	220	109	5158	195
54			1,62	1,75	310	180	151	202	137	5690	287
55			1,633	1,761	85	119	94	220	276	4844	386
56			1,65	1,776	195	99	158	135	278	4849	346
57			1,684	1,807	103	170	125	106	120	4477	388
58			1,7	1,825	127	112	168	67	84	4340	207
59			1,717	1,842	98	47	99	84	75	1996	197
60			1,734	1,86	334	149	145	110	125	6474	450
61			1,765	1,896	139	110	103	68	96	4649	292
62			1,78	1,915	147	90	103	145	161	5792	503
63	H2	Chambira	1,795	1,933	254	149	116	139	105	8456	576
64			1,815	1,953	174	203	190	187	203	12707	684
65			1,832	1,965	200	110	165	140	116	4726	374
66			1,847	1,991	106	227	152	210	183	7382	442
67			1,868	2,011	153	70	83	75	207	3740	284
68			1,888	2,024	113	92	95	96	135	3291	136
69			1,905	2,042	106	114	121	158	125	9318	622
70			1,912	2,067	123	66	81	96	97	5089	273
71			1,947	2,086	146	72	94	93	138	5739	498
72			1,957	2,096	67	114	119	137	148	14184	684
73			1,967	2,106	102	86	73	82	72	4829	339
74			1,977	2,116	165	134	108	139	123	6870	240
75			1,987	2,126	96	74	118	83	104	4915	350
76			1,997	2,136	60	66	77	101	44	2707	193
77			2,019	2,154	41	60	47	41	76	8178	813
78			2,041	2,157	96	49	82	94	51	2266	126
79			2,065	2,178	126	94	77	92	80	1945	175
80			2,071	2,209	123	109	205	101	199	5396	380
81			2,094	2,24	67	86	88	103	79	2727	197
82			2,113	2,256	69	42	60	62	72	4323	148
83	H1	Pozo	2,143	2,28	65	81	98	100	84	1907	72
84			2,158	2,321	128	226	84	127	159	4490	196

85		Present day surface							11917	620
86		Present day surface							43900	2120

351

352 **FIGURES CAPTIONS**

353 Figure 1: A. Amazon Basin drainage outline over SRTM digital elevation model and
 354 HydroSHEDS river network (EO, NASA). B. Major world rivers yield (drainage area >10³ km²)
 355 as a function of drainage area (Syvitski et al., 2005). C. Comparison of two different satellite
 356 images over the Rio Ucayali (UAVSAR data courtesy NASA/JPL-Caltech, Landsat imagery
 357 courtesy of NASA Goddard Space Flight Center and U.S. Geological Survey), note the resolution
 358 over the UAVSAR image that highlights the detailed architecture of the meanders and lateral
 359 accretion formed by the Rio Ucayali.

360 Figure 2: (A) Example of the Marañón Basin Cenozoic infill from the (B) seismic line that
 361 illustrates the regional geometry across the Marañón Basin from the foothills of the Andes (SW)
 362 to the Iquitos Arch (NE) and (C) detailed lithologic and stratigraphic information from a well
 363 located south of the regional cross section. Note the thickness of the Chambira Formation that
 364 spans from Eocene to the Upper Oligocene, the aggrading pattern is associated with floodplain
 365 and fluvial channel and sand sheets stacking. The Neogene Pebas, Marañón and Corrientes
 366 Formations show more variations in lithological content.

367 Figure 3: (A) Seismic reflection amplitude and stratigraphy of the Marañón Basin Cenozoic infill.
 368 (B) The relatively continuous to discontinuous character of the reflection strength is enhanced by
 369 the sweetness attribute, thick sands are associated with high sweetness values (i.e. blue or yellow
 370 colors). (C and D) The phase and thin-bed attribute are used to highlight the pinch-out and tuning

371 of the channels and its infill. The colored triangles are selected horizons displayed in Figure 6.

372 Location of the seismic line is located in Figure 2A and in Figure 6.

373 Figure 4: Quantitative geomorphologic measures along a horizon slice with sweetness attribute

374 display. Channel width (W), meander belt width (MBW), channel length on one wavelength (La),

375 meander wavelength (ML), and radius of curvature (RC). Sinuosity is calculated by channel

376 length divided by meander wavelength.

377 Figure 5: Seismic facies observed and interpreted in the Marañón Basin within the Cenozoic

378 infill. All seismic sections and plan views of the facies are scaled with the same amplitude values

379 and vertical/horizontal scales.

380 Figure 6: Evolution of the fluvial patterns observed and interpreted on colored blended spectral

381 decomposition horizons highlighting the main changes in the stratigraphy of the Cenozoic

382 sequence of the Marañón Basin. The RGB compositions show frequency 39, 32, and 29 Hz

383 respectively. The color code for each slice A to H corresponds to the arrows on the seismic

384 section displayed in Figure 3A. The RBG blend horizons are displayed from shallower part to

385 deep part of the basin. The white line drawing is associated to features related to fluvial

386 geometries, main channels and extensive fluvial features are interpreted following facies scheme

387 in Figure 5.

388 Figure 7: Statistical analysis of quantified fluvial channel width from the Cenozoic record of the

389 Marañón Basin. Channel width classification is from Gibling (2006), narrow to medium channels

390 correspond to 100 m width.

391 Figure 8: Statistical analysis of sinuosity from quantified meanders of the Cenozoic record of the
392 Marañón Basin. Classification of alluvial channels by sediment load is based on Schumm (1985).
393 The cutoffs used to differentiate the type of channels based on sinuosity are 1.3 and 2.

394 Figure 9: Stratigraphic evolution of channels width, belt width, sinuosity and paleocurrents from
395 the Cenozoic record of the Marañón Basin. This reconstruction is based on observation,
396 interpretation and quantification of 84 seismic stratigraphic surfaces extracted in the seismic
397 reflection 3D cube.

398 Figure 10: (A) Present day surface of the western part of the Amazon Basin. Inset of fluvial
399 systems from the proximal Rio Pastaza and the Napo-Pastaza Megafan to intermediate Rio
400 Ucayali south of Iquitos. (B) Example of 3D seismic survey used for this study, note the areal
401 extent of a survey compared to the natural features observed at its edge, the rivers flow from NW
402 to SE. (C) Example of meandering and laterally incising paleodrainage, in relation to the NW-SE
403 plunging Iquitos Arch. (D) Low land and flood plain in the Pastaza-Corrientes transition band
404 north of the Rio Marañón, note the various abandoned splays and the amount of meandering
405 channels. (E) Encased Rio Ucayali meandering channel with large point bar and cut off loops.
406 Note the variety of properties of the various channels and their lateral lowland landscapes. DEM
407 from B to E are at the same horizontal scale, vertical relief is lows for dark and bright for highs.
408 DEM are sourced from SRTM (NASA), UAVSAR data courtesy NASA/JPL-Caltech, *Landsat*
409 imagery *courtesy of* NASA Goddard Space Flight Center and U.S. Geological Survey.

410 Figure 11: Comparative fluvial views from detailed (A) UAVSAR over the Rio Ucayali, (B)
411 Landsat over rivers and streams from the Amazon Basin and (C) 3D seismic interpreted spectral
412 decomposition images/maps from the Marañón Basin. Note the 5x5 km black square that allows

413 comparison of architectural elements from the three different sourced images. DEM are sourced
414 from SRTM (NASA), UAVSAR data courtesy NASA/JPL-Caltech, *Landsat* imagery courtesy of
415 NASA Goddard Space Flight Center and U.S. Geological Survey. Fluvial features: channel, bars,
416 meanders, lateral accretion, oxbow lake (ox. l).

417 REFERENCES

- 418 Alexander, J. (1993). A discussion on the use of analogues for reservoir geology. Geological Society,
419 London, Special Publications, 69(1), 175–194.
- 420 Allen, P. (2017). *Sediment Routing Systems: The Fate of Sediment from Source to Sink*. Cambridge:
421 Cambridge University Press. doi:10.1017/9781316135754
- 422 Alqahtani, F. A., Jackson, C. A.-L, Johnson, H.D., Som, M. R. B., 2017. Controls On the Geometry and
423 Evolution of Humid-Tropical Fluvial Systems: Insights From 3D Seismic Geomorphological Analysis of
424 the Malay Basin, Sunda Shelf, Southeast Asia. *Journal of Sedimentary Research*, 87 (1), 17–40.
- 425 Ashworth, P. J., Lewin, J., 2012. How do big rivers come to be different? *Earth-Science Reviews*, 114(1–
426 2), 84–107.
- 427 Baby, P., M. Rivadeneira, R. Barragán, F. Christophoul, 2013. Thick-skinned tectonics in the Oriente
428 foreland basin of Ecuador, In: Nemčok M., Mora A. R., Cosgrove J. W. (eds) *Thick-Skin-Dominated*
429 *Orogens: From Initial Inversion to Full Accretion*, Geological Society, London, Special Publications, 377,
430 59–76.
- 431 Bernal, C., Christophoul, F., Darrozes, J., Soula, J.-C., Baby, P., & Burgos, J. (2011). Late
432 Glacial and Holocene avulsions of the Rio Pastaza Megafan (Ecuador--Peru): frequency and
433 controlling factors. *International Journal of Earth Sciences*, 100(7), 1759–1782.
434 <https://doi.org/10.1007/s00531-010-0555-9>
- 435 Bridge, J. S., Tye, R. S., 2000. Interpreting the Dimensions of Ancient Fluvial Channel Bars, Channels,
436 and Channel Belts from Wireline-Logs and Cores. *AAPG Bulletin*, 84(8), 1205–1228.
- 437 Callède, J., Guyot, J. L., Ronchail, J., L'Hôte, Y., Niel, H., de Oliveira, E., 2004. Evolution du débit de
438 l'Amazone à Óbidos de 1903 à 1999/Evolution of the River Amazon's discharge at Óbidos from 1903 to
439 1999. *Hydrological Sciences Journal*, 49, 85–97.
- 440 Calvès, G., Calderón, Y., Enriquez, C. H., Brusset, S., Santini, W., & Baby, P. (2018). Mass balance of
441 cenozoic andes-amazon source to sink system—marañón basin, Peru. *Geosciences (Switzerland)*,
442 8(5). <https://doi.org/10.3390/geosciences8050167>
- 443 Clift, P.D., Olson, E.D., Lechnowskyj, A., Moran, M.G., Barbato, A., & Lorenzo, J.M., (2018). Grain-size
444 Variability within a Mega-scale Point Bar System, False River, Louisiana. *Sedimentology*.
445 doi:10.1111/sed.12528.

- 446 Constantine, J. A., Dunne, T., Ahmed, J., Legleiter, C., & Lazarus, E. D., 2014. Sediment supply as a
447 driver of river meandering and floodplain evolution in the Amazon Basin. *Nature Geosci*, 7(12), 899–903.
- 448 Dumont, J. F., Deza, E., & Garcia, F. (1991). Morphostructural provinces and neotectonics in the
449 Amazonian lowlands of Peru. *Journal of South American Earth Sciences*, 4(4), 373–381.
450 [https://doi.org/https://doi.org/10.1016/0895-9811\(91\)90008-9](https://doi.org/https://doi.org/10.1016/0895-9811(91)90008-9)
- 451 El-Mowafy, H. Z., Marfurt, K. J., 2016. Quantitative seismic geomorphology of the middle Frio fluvial
452 systems, south Texas, United States. *AAPG Bulletin*, 100(4), 537–564.
- 453 Ethridge, F.G., Schumm, S.A., 2007. Fluvial seismic geomorphology: a view from the surface: Geological
454 Society, London, Special Publications, 277, 205–222.
- 455 Espurt, N., Baby, P., Brusset, S. Roddaz, M., Hermoza, W., Regard, V., Antoine, P.-O., Salas-Gismondi,
456 R., Bolaños, R., 2007. How does the Nazca Ridge subduction influence the modern Amazonian foreland
457 basin?. *Geology*, 35, 515–518.
- 458 Figueiredo, J., Hoorn, C., Van der Ven, P., Soares, E., 2009. Late Miocene onset of the Amazon River and
459 the Amazon deep-sea fan: Evidence from the Foz do Amazonas Basin. *Geology*, 37, 619–622.
- 460 Fisher, S. G., Heffernan, J. B., Sponseller, R. A., & Welter, J. R. (2007). Functional
461 ecomorphology: Feedbacks between form and function in fluvial landscape ecosystems.
462 *Geomorphology*, 89(1), 84–96.
463 <https://doi.org/https://doi.org/10.1016/j.geomorph.2006.07.013>
- 464
- 465 Flament, N., Gurnis, M., Müller, R. D., Bower, D. J., Husson, L., 2015. Influence of subduction history on
466 South American topography. *Earth and Planetary Science Letters*, 430(Supplement C), 9–18.
- 467 Gaillardet, J., Dupre, B., Allegre, C. J., Négrel, P., 1997. Chemical and physical denudation in the
468 Amazon River Basin. *Chemical Geology*, 142, 141–173.
- 469 Gibling, M. R., 2006. Width and Thickness of Fluvial Channel Bodies and Valley Fills in the Geological
470 Record: A Literature Compilation and Classification. *Journal of Sedimentary Research*, 76, 731–770.
- 471 Gorini, C., Haq, B.U., dos Reis, A.T., Silva, C.G., Cruz, A., Soares, E., Grangeon, D., 2014. Late Neogene
472 sequence stratigraphic evolution of the Foz do Amazonas Basin, Brazil. *Terra Nova* 26, 179–185.
- 473 Gross, M., Piller, W. E., Ramos, M. I., & Douglas da Silva Paz, J. (2011). Late Miocene
474 sedimentary environments in south-western Amazonia (Solimões Formation; Brazil).
475 *Journal of South American Earth Sciences*, 32(2), 169–181.
476 <https://doi.org/10.1016/j.jsames.2011.05.004>
- 477 Hardage, B. A., Remington, R. L., 1999. 3-D seismic stratal-surface concepts applied to the interpretation
478 of a fluvial channel system deposited in a high-accommodation environment. *Geophysics*, 64, 609–620.
- 479 Hart, B. S. 2008. Channel detection in 3-D seismic data using sweetness. *AAPG Bulletin*, 92, 733–742.

- 480 Hermoza, W., Brusset, S., Baby, P., Gil, W., Roddaz, M., Guerrero, N., Bolaños, R., 2005. The Huallaga
481 foreland basin evolution: Thrust propagation in a deltaic environment, northern Peruvian Andes. *Journal*
482 *of South American Earth Sciences*, 19(1), 21–34.
- 483 Hoorn, C., Wesselingh, F. P., Ter Steege, H., Bermudez, M. A., Mora, A., Sevink, J., Antonelli, A., 2010.
484 Amazonia through time: Andean uplift, climate change, landscape evolution, and biodiversity. *Science*,
485 330, no.6006, 927–931.
- 486 Hoorn, C., Bogotá-A, G.R., Romero-Baez, M., Lammertsma, E.I., Flantua, S.G.A., Dantas, E.L., Dino, R.,
487 do Carmo, D.A., Chemale Jr, F., 2017. The Amazon at sea: Onset and stages of the Amazon River from a
488 marine record, with special reference to Neogene plant turnover in the drainage basin. *Glob. Planet.*
489 *Change* 153, 51–65.
- 490 Hubbard, S. M., Smith, D. G., Nielsen, H., Leckie, D. A., Fustic, M., Spencer, R. J., Bloom, L., 2011.
491 Seismic geomorphology and sedimentology of a tidally influenced river deposit, Lower Cretaceous
492 Athabasca oil sands, Alberta, Canada. *AAPG Bulletin*, 95, 1123–1145.
- 493 Hurtado, C., Roddaz, M., Santos, R. V., Baby, P., Antoine, P.-O., Dantas, E. L., 2018 Cretaceous-early
494 Paleocene drainage shift of Amazonian rivers driven by Equatorial Atlantic Ocean opening and Andean
495 uplift as deduced from the provenance of northern Peruvian sedimentary rocks (Huallaga basin).
496 *Gondwana Research* 63, 152-168, doi:10.1016/j.gr.2018.05.012.
- 497 Jaramillo, C., Romero, I., D’Apolito, C., Bayona, G., Duarte, E., Louwye, S., Escobar, J., Luque, J.,
498 Carrillo-Briceño, J. D., Zapata, V., Mora, A., Schouten, S., Zavada, M., Harrington, G., Ortiz, J.,
499 Wesselingh, F. P., 2017. Miocene flooding events of western Amazonia. *Science Advances*, 3(5), doi:
500 10.1126/sciadv.1601693
- 501 Kröhling, D. M., 2017. Analysis of the Quaternary climatic and tectonic forcing along some different
502 tectonic settings of South America. *Quaternary International*, 438, 1–3.
- 503 Latrubesse, E. M., 2015. Large rivers, megafans and other Quaternary avulsive fluvial systems: A
504 potential “who’s who” in the geological record. *Earth-Science Reviews*, 146, 1–30.
- 505 Latrubesse, E. M., Cozzuol, M., da Silva-Caminha, S. A. F., Rigsby, C. A., Absy, M. L., Jaramillo, C.,
506 2010. The Late Miocene paleogeography of the Amazon Basin and the evolution of the Amazon River
507 system. *Earth-Science Reviews*, 99(3), 99–124.
- 508 Lewin, J., Ashworth, P. J., 2014. Defining large river channel patterns: Alluvial exchange and plurality.
509 *Geomorphology*, 215, 83–98.
- 510 Martin, R., 1966. Paleogeomorphology and its application to exploration for oil and gas (with examples
511 from western Canada). *AAPG Bulletin*, 50, 2277–2311.
- 512 Maynard, J. R., Feldman, H. R., Alway, R., 2010. From bars to valleys: the sedimentology and seismic
513 geomorphology of fluvial to estuarine incised-valley fills of the Grand Rapids Formation (Lower
514 Cretaceous), Iron River Field, Alberta Canada. *Journal of Sedimentary Research*, 80, 611–638.
- 515 Miall, A. D., 2000. Basin-Mapping Methods. In: *Principles of Sedimentary Basin Analysis*. Springer,
516 Berlin, Heidelberg
- 517 Miall, A. D., 2002. Architecture and sequence stratigraphy of Pleistocene fluvial systems in the Malay
518 Basin, based on seismic time-slice analysis. *AAPG Bulletin*, 86, no.7, 1201–1216.

- 519 Miall, A. D., 2006. How do we identify big rivers? And how big is big?. *Sedimentary Geology*, 186, 39–
520 50.
- 521 Miall, A. D., 2014. *Fluvial Depositional Systems*, Springer, 316 p.
- 522 Milliman, J. D., Syvitski, J. P., 1992. Geomorphic/tectonic control of sediment discharge to the ocean: the
523 importance of small mountainous rivers. *The Journal of Geology*, 100, 525–544.
- 524 Partyka, G., Gridley, J., Lopez, J., 1999. Interpretational applications of spectral decomposition in
525 reservoir characterization. *The Leading Edge*, 18, 353–360.
- 526 Posamentier, H. W., 2000. Seismic stratigraphy into the next millennium; a focus on 3D seismic data:
527 AAPG Annual Conference, New Orleans, LA, 16-19 April, 2000, A118.
- 528 Posamentier, H. W., 2001. Lowstand alluvial bypass systems: incised vs. unincised. *AAPG Bulletin*, 85,
529 1771–1793.
- 530 Posamentier, H. W., 2003. Depositional elements associated with a basin floor channel-levee system: case
531 study from the Gulf of Mexico. *Marine and Petroleum Geology*, 20, 677–690.
- 532 Potter, P. E., 1978. Significance and Origin of Big Rivers. *The Journal of Geology*, 86(1), 13–33.
- 533 Qi'an, M., Shun, Z., Guoxin, S., Xiuli, F., Chao, W., Yao, S., 2015. A seismic geomorphology study of
534 the fluvial and lacustrine-delta facies of the Cretaceous Quantou-Nenjiang Formations in Songliao Basin,
535 China. *Marine and Petroleum Geology*, 78, 836–847.
- 536 Räsänen, M. E., Salo, J. S., Kalliola, R. J., 1987. Fluvial Perturbance in the Western Amazon Basin:
537 Regulation by Long-Term Sub-Andean Tectonics. *Science*, 238(4832), 1398–1401.
- 538 Räsänen, M. E., Salo, J. S., Jungner, H., Pittman, L. R., 1990. Evolution of the Western Amazon Lowland
539 Relief: impact of Andean foreland dynamics. *Terra Nova*, 2(4), 320–332.
- 540 Räsänen, M., Neller, R., Salo, J., Jungner, H., 1992. Recent and ancient fluvial deposition systems in the
541 Amazonian foreland basin, Peru. *Geological Magazine*, 129(3), 293–306.
- 542 Rebata H., L. A., Räsänen, M. E., Gingras, M. K., Vieira, V., Barberi, M., & Irion, G. (2006).
543 Sedimentology and ichnology of tide-influenced Late Miocene successions in western
544 Amazonia: The gradational transition between the Pebas and Nauta formations. *Journal of*
545 *South American Earth Sciences*, 21(1–2), 96–119.
546 <https://doi.org/10.1016/j.jsames.2005.07.011>
- 547 Reijenstein, H. M., Posamentier, H. W., Bhattacharya, J. P., 2011. Seismic geomorphology and high-
548 resolution seismic stratigraphy of inner-shelf fluvial, estuarine, deltaic, and marine sequences, Gulf of
549 Thailand. *AAPG Bulletin*, 95, 1959–1990.
- 550 Roddaz, M., Baby, P., Brusset, S., Hermoza, W., Darrozes, J. M., 2005. Forebulge dynamics and
551 environmental control in Western Amazonia. The case study of the Arch of Iquitos (Peru):
552 Tectonophysics, 399, 87–108.
- 553 Roddaz, M., Hermoza, W., Mora, A., Baby, P., Parra, M., Christophoul, F., Brusset, S., Espurt, N., 2010.
554 Cenozoic Sedimentary Evolution of the Amazonian Foreland Basin System, in: Hoorn, C., Wesselingh,
555 F.P. (Eds.), *Amazonia: Landscape and Species Evolution*. Wiley-Blackwell Publishing Ltd., pp. 61–88

- 556 Rodríguez Tribaldos, V., White, N. J., Roberts, G. G., Hoggard, M. J., 2017. Spatial and temporal uplift
557 history of South America from calibrated drainage analysis. *Geochem. Geophys. Geosyst.*, 18,
558 doi:10.1002/2017GC006909.
- 559 Sarzalejo, S., Hart, B. S., 2006. Stratigraphy and lithologic heterogeneity in the Mannville Group
560 (southeast Saskatchewan) defined by integrating 3-D seismic and log data. *Bulletin of Canadian Petroleum
561 Geology*, 54, 138–151.
- 562 Schumm, S. A., 1985. Patterns of Alluvial Rivers. *Annual Review of Earth and Planetary Sciences*, 13(1),
563 5–27.
- 564 Schumm, S. A., 2005. *River Variability and Complexity*. Cambridge University Press, Cambridge.
- 565 Shephard, G. E., Müller, R. D., Liu, L., Gurnis, M., 2010. Miocene drainage reversal of the Amazon River
566 driven by plate–mantle interaction. *Nature Geoscience*, 3, 870–875.
- 567 Sheriff, R. E., 1992. Vertical and Lateral Seismic Resolution and Attenuation: Part 7. Geophysical
568 Methods. In D. Morton-Thompson and A. M. Woods, eds., *Development Geology Reference Manual*,
569 AAPG Methods in Exploration Series, 10, 388–389.
- 570 Southwood, T.R.E., 1977. Habitat, the templet for ecological strategies. *Journal of Animal Ecology* 46,
571 337–365.
- 572 Stokes, M. F., Goldberg, S. L., & Perron, J. T. (2018). Ongoing River Capture in the Amazon.
573 *Geophysical Research Letters*, 45(11), 5545–5552. <https://doi.org/10.1029/2018GL078129>
- 574
- 575 Syvitski, J.P.M., Kettner, A.J., Correggiari, A., Nelson, B.W., 2005. Distributary channels and their
576 impact on sediment dispersal. *Marine Geology*, 222–223, 75–94.
- 577 Taner, M. T., Sheriff, R. E., 1977. Application of amplitude, frequency, and other attributes to
578 stratigraphic and hydrocarbon determination: In: AAPG Memoir 26: Seismic Stratigraphy-Applications to
579 Hydrocarbon Exploration (Ed. C.E. Payton), 301–327.
- 580 Taner, M., Koehler, F., Sheriff, R., 1979. Complex seismic trace analysis. *Geophysics*, 44(6), 1041–1063.
- 581 Taner, M.T., 2003. Attributes revisited. <http://www.rocksolidimages.com/attributes-revisited>
- 582 van Soelen, E.E., Kim, J.-H., Santos, R.V., Dantas, E.L., Vasconcelos de Almeida, F., Pires, J.P., Roddaz,
583 M., Sinninghe Damsté, J.S., 2017. A 30 Ma history of the Amazon River inferred from terrigenous
584 sediments and organic matter on the Ceará Rise. *Earth Planet. Sci. Lett.* 474, 40–48.
- 585 Wang, Z., Yin, C., Fan, T., X., Lei, 2012. Seismic geomorphology of a channel reservoir in lower
586 Minghuazhen Formation, Laizhouwan subbasin, China. *Geophysics*, 77, 187–195.
- 587 Weber, K. J., 1992. The Use of 3-D Seismic in Reservoir Geological Modelling. In: *The Geological
588 Modelling of Hydrocarbon Reservoirs and Outcrop Analogues*. Blackwell Publishing Ltd. 181–188.
- 589 Weissmann, G. S., Hartley, A. J., Scuderi, L. A., Nichols, G. J., Owen, A., Wright, S., Felicia, A. L.,
590 Holland, F., Anaya, F. M. L., 2015. Fluvial geomorphic elements in modern sedimentary basins and their
591 potential preservation in the rock record: A review. *Geomorphology*, 250, 187–219.

592 Wesselingh, F. P., Hoorn, C., Kroonenberg, S. B., Antonelli, A., Lundberg, J. G., Vonhof, H. B.,
593 Hooghiemstra, H., 2009. On the origin of Amazonian landscapes and biodiversity: a synthesis. In C.
594 Hoorn and F. P. Wesselingh, eds, Amazonia: Landscape and Species Evolution: A look into the past,
595 Wiley-Blackwell Publishing Ltd., Oxford, UK. 419–431.

596 Westaway, R., 2006. Late Cenozoic sedimentary sequences in Acre state, southwestern Amazonia: Fluvial
597 or tidal? Deductions from the IGCP 449 fieldtrip. *Journal of South American Earth Sciences*, 21(1), 120–
598 134.

599 Wood, L. J., 2007. Quantitative seismic geomorphology of Pliocene and Miocene fluvial systems in the
600 northern Gulf of Mexico, USA. *Journal of Sedimentary Research*, 77, 713–730.

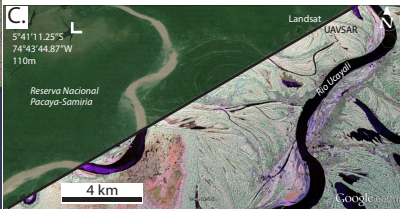
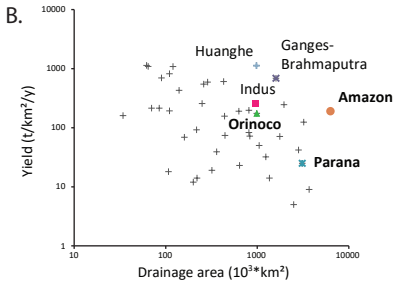
601 Zeng, H., 2007. Seismic imaging for seismic geomorphology beyond the seabed: potentials and
602 challenges. *Geological Society, London, Special Publications*, 277, 15–28.

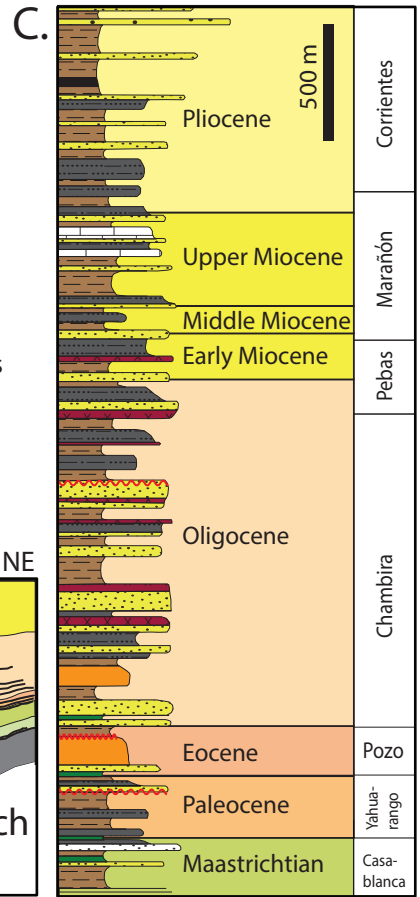
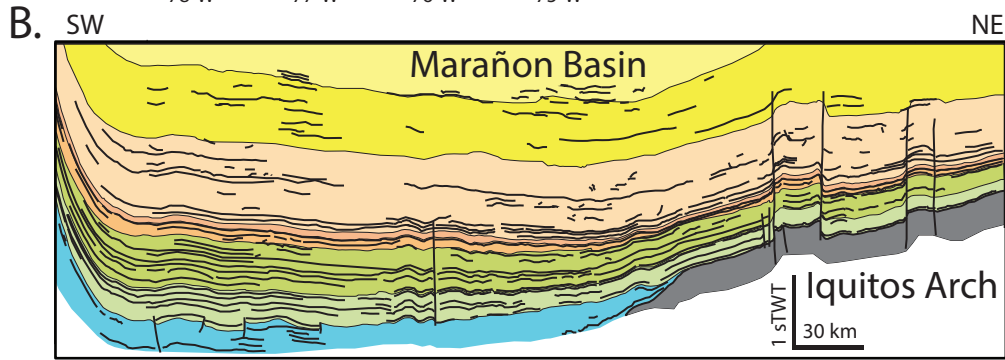
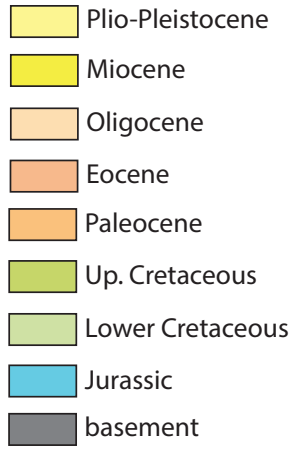
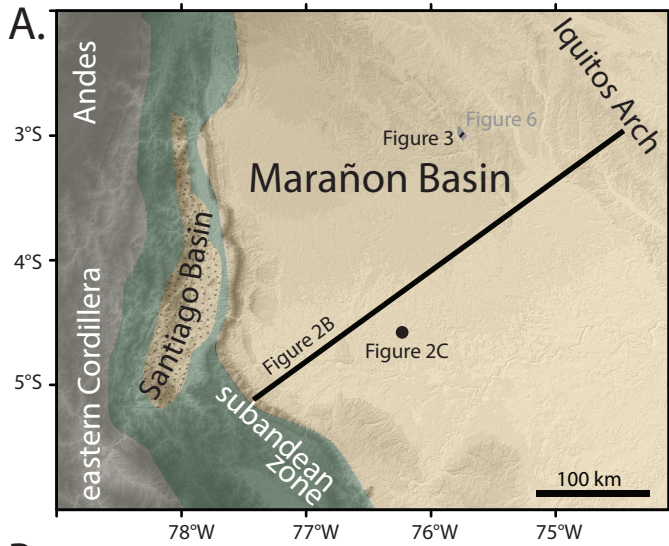
603 Zhuo, H., Wang, Y., Shi, H., He, M., Chen, W., Li, H., Wang, Y., Yan, W., 2015. Contrasting fluvial
604 styles across the mid-Pleistocene climate transition in the northern shelf of the South China Sea: Evidence
605 from 3D seismic data. *Quaternary Science Reviews*, 129, 128–146.

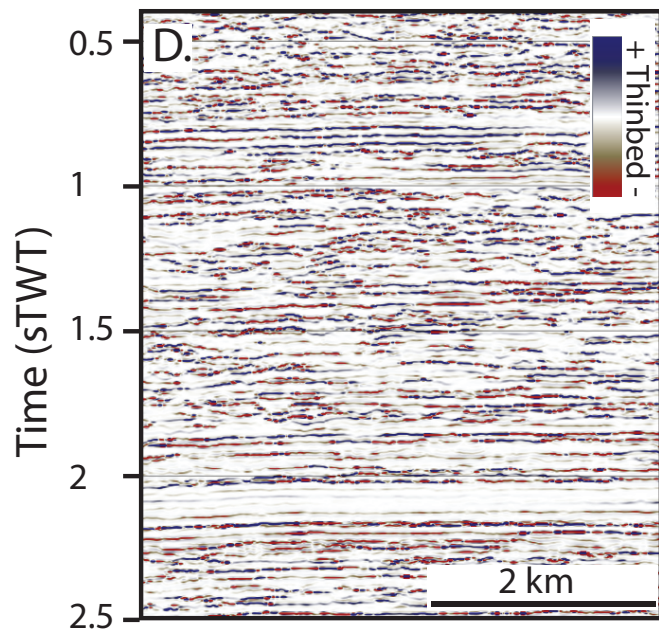
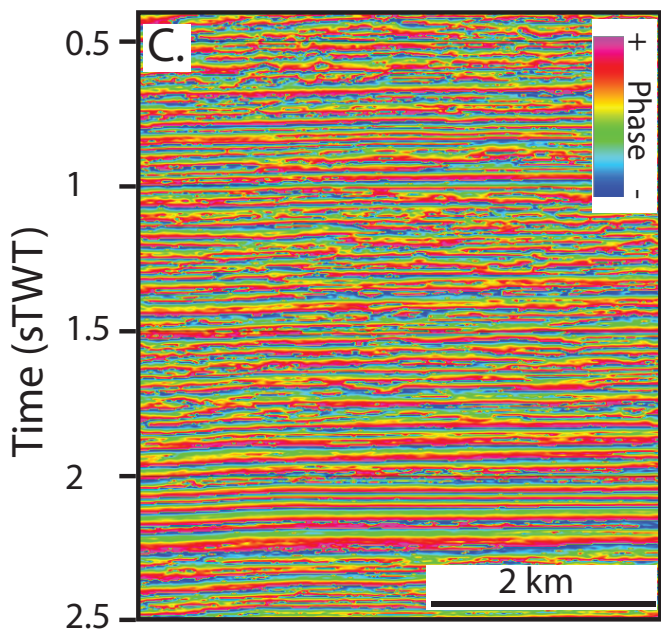
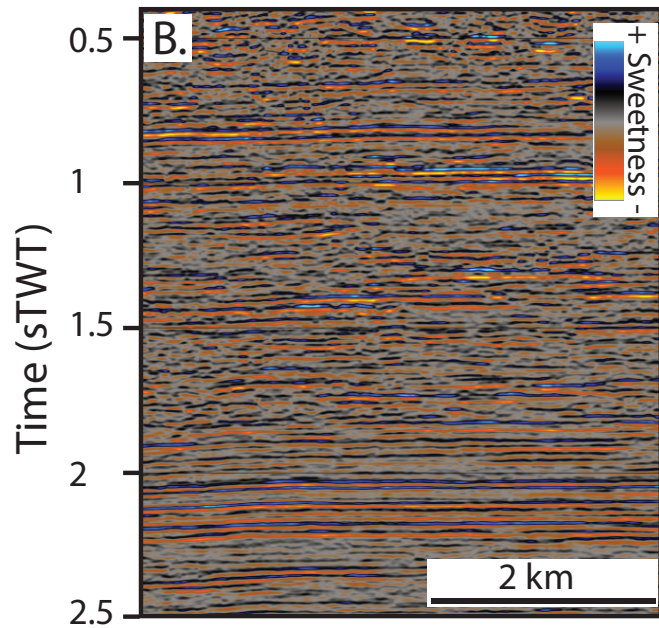
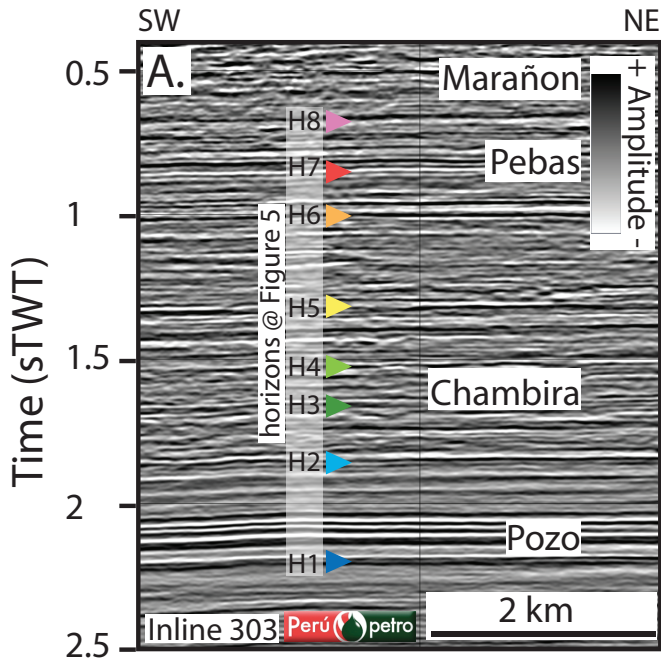
606 **SUPPLEMENTARY DATA:**

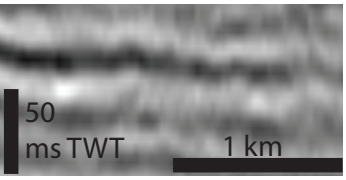
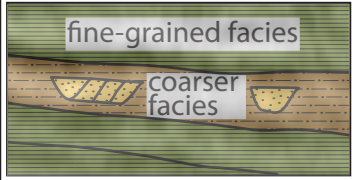
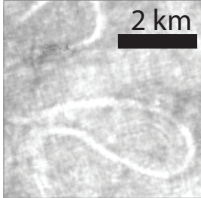
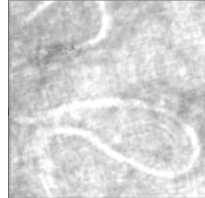
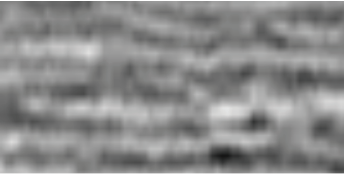
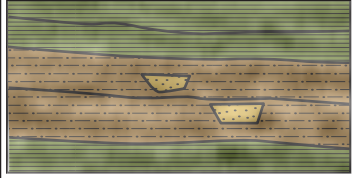
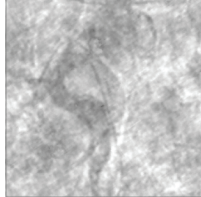
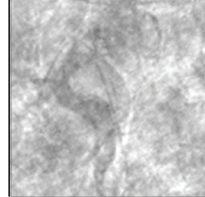
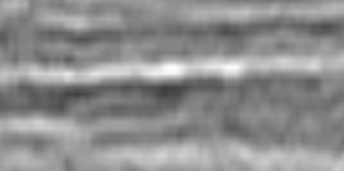

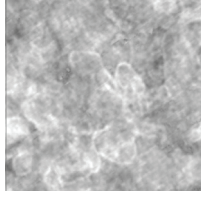
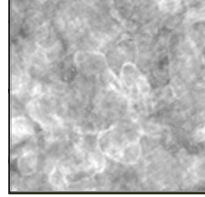

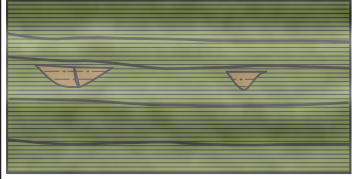
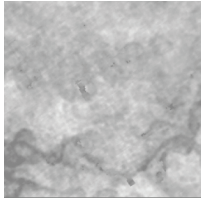
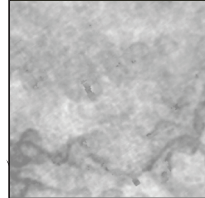

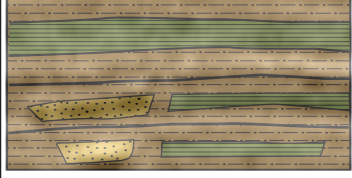
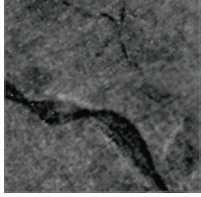
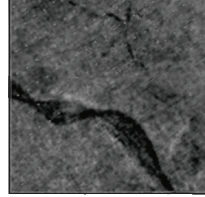

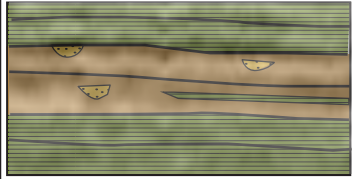
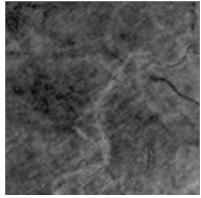
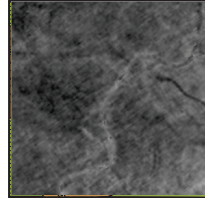
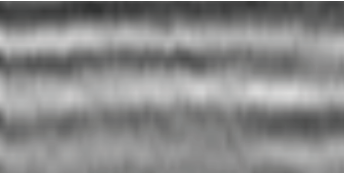
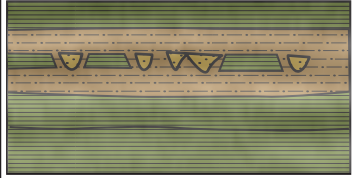
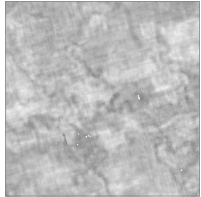
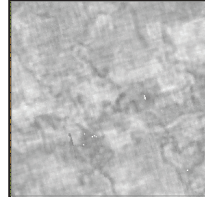

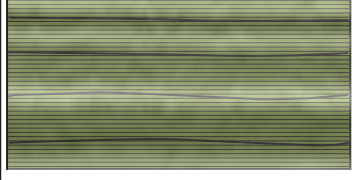


Name	Hor_slice_Amp.mpg
Caption/description	Animated seismic amplitude horizon slicing from surface (topography) to depth. The seismic amplitude horizon slices are displayed with a black (positive) to white (negative) scale bar.
Type	Video.
Format	MPG.
Duration	261 seconds.
Frame size	600x300 pixels.
Producer	Windows live movie maker and conversion from WMV to MPG file.

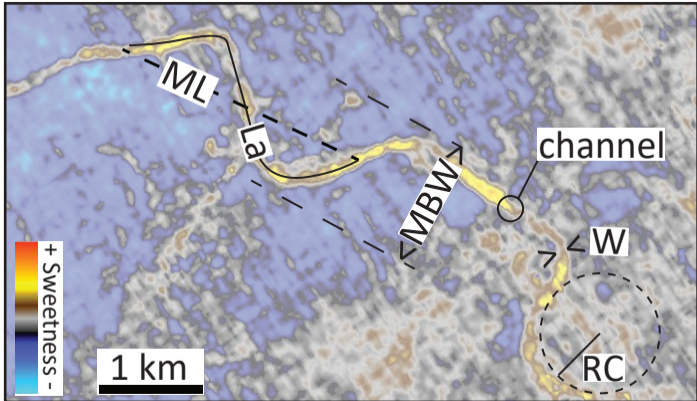
607

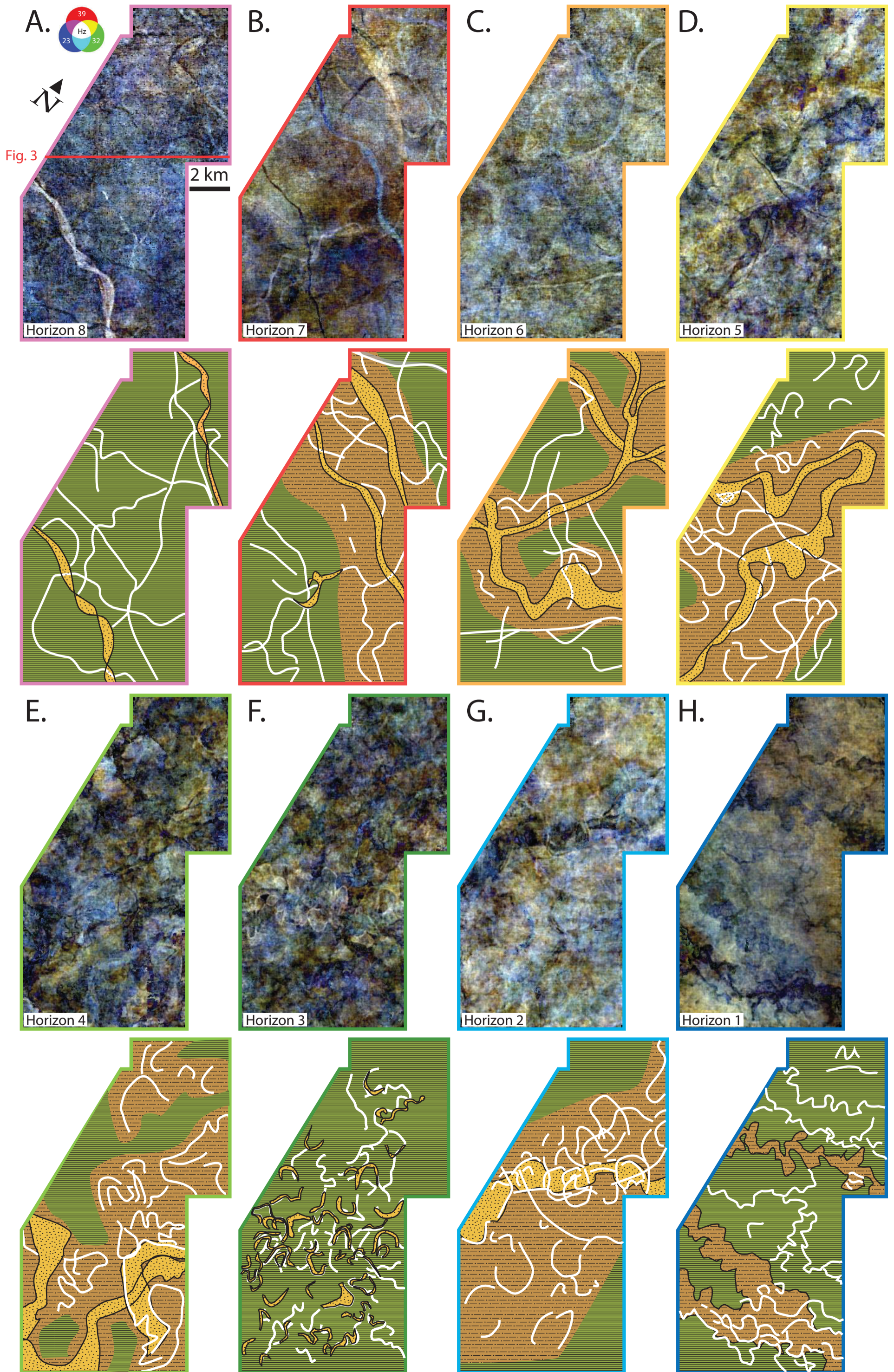


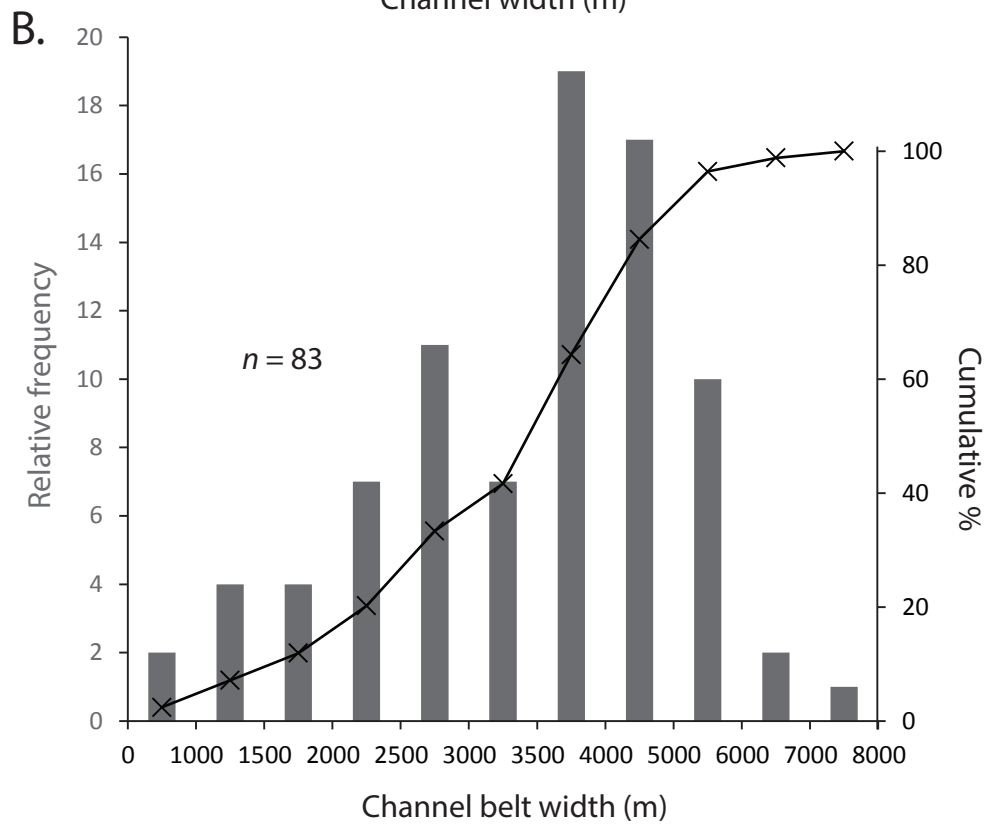
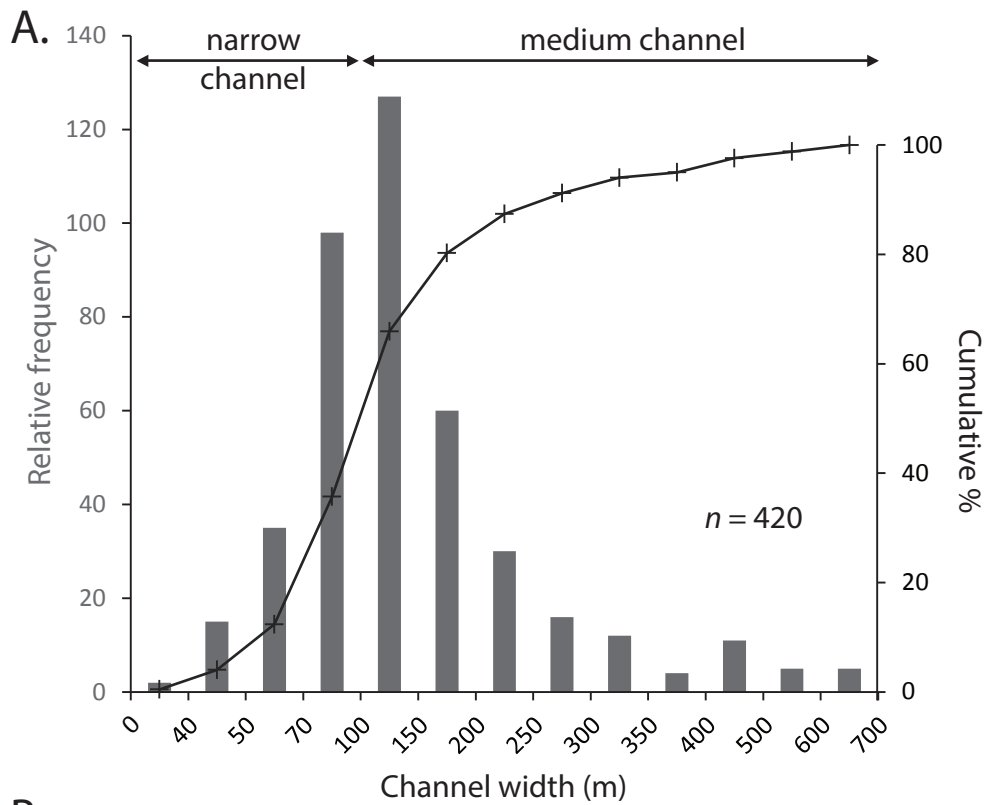


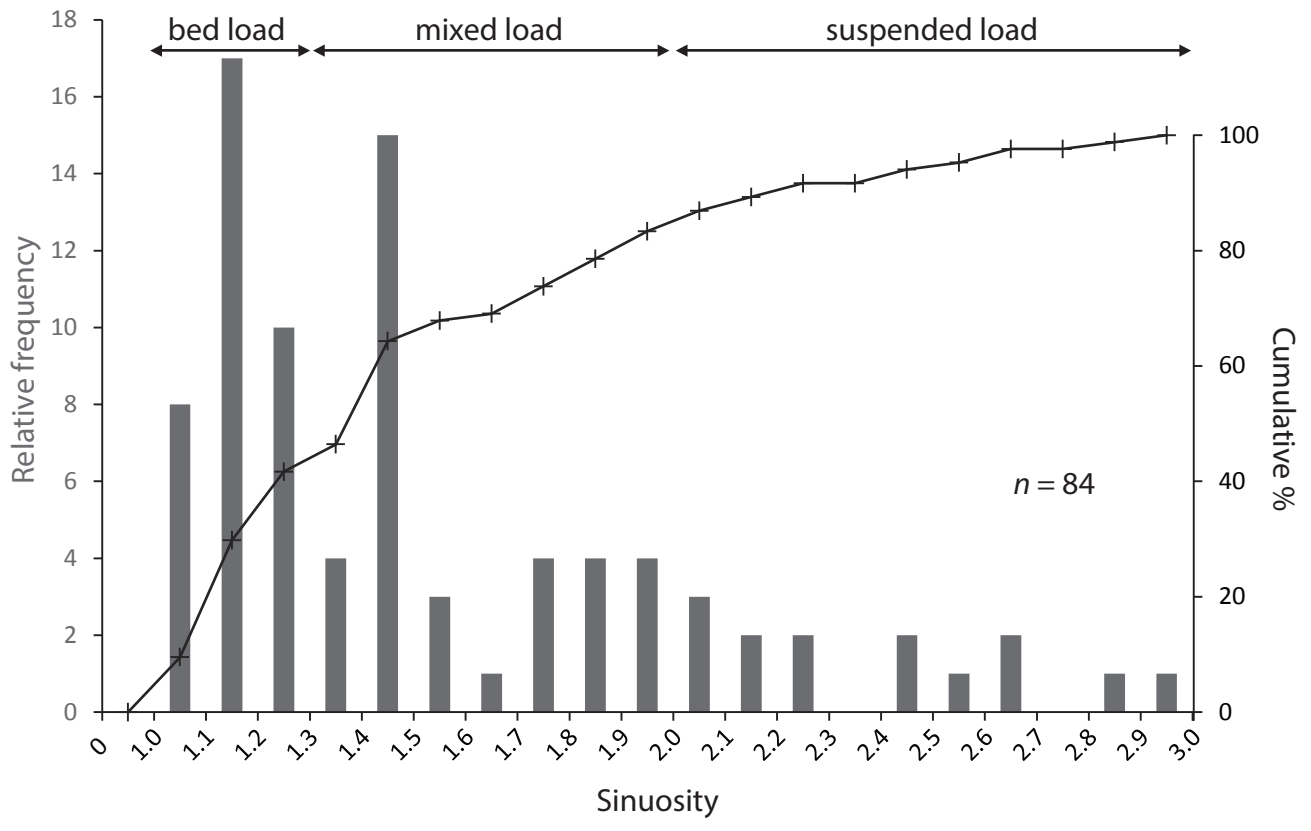


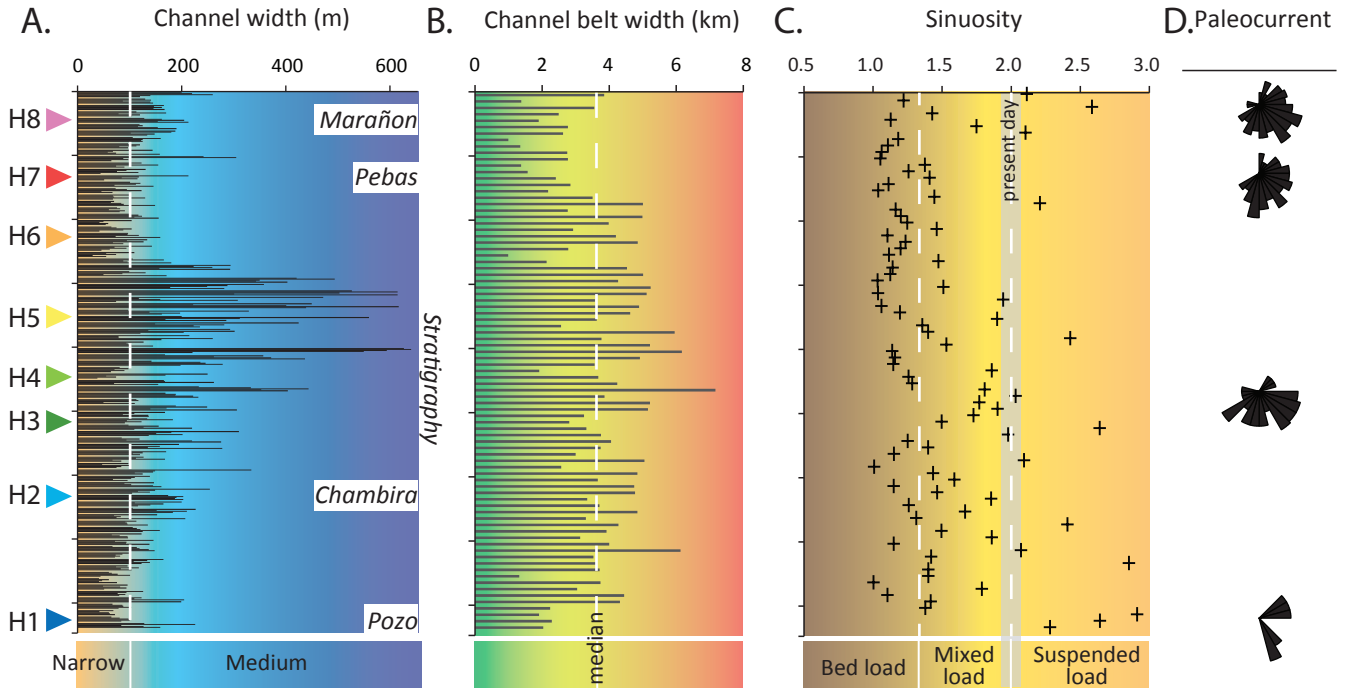
Seismic facies	Seismic section + Amplitude -	Interpretation	Plan view + Amplitude -	Interpretation	Reflection character/Sedimentologic interpretation
SF1					<p>moderate to high amplitude, continuous reflection</p> <p>high amplitude related to channel</p> <p>peak frequency : 30 Hz</p> <p>channel width 100-200 m</p> <p>fluvial feature : meanders, high sinuosity and lateral accretion</p>
SF2					<p>low to moderate amplitude, moderate continuity of reflection</p> <p>mixed amplitude change within larger channels</p> <p>peak frequency : 32 Hz</p> <p>channel width 70-650 m</p> <p>fluvial feature : meanders, moderate sinuosity and bars</p>
SF3					<p>low to moderate amplitude, moderate continuity of reflection</p> <p>mixed amplitude change of channel</p> <p>peak frequency : 32 Hz</p> <p>channel width 70-270 m</p> <p>fluvial feature : meanders, moderate sinuosity and bars</p>
SF4					<p>low amplitude, shingled to continuous reflection</p> <p>lowest amplitude related to channel</p> <p>peak frequency : 17 Hz</p> <p>channel width 80-300 m</p> <p>fluvial feature : meanders, low to moderate sinuosity</p>
SF5					<p>low to high amplitude, continuous reflection</p> <p>high amplitude related to channel</p> <p>peak frequency : 27 Hz</p> <p>channel width 80-300 m</p> <p>fluvial feature : meanders, low sinuosity and lateral accretion</p>
SF6					<p>low to high amplitude, shingled to continuous reflection</p> <p>high amplitude related to channel</p> <p>peak frequency : 45 Hz</p> <p>channel width 40-360 m</p> <p>fluvial feature : meanders, low sinuosity, stacking and cross-cutting channels</p>
SF7					<p>low to moderate amplitude, continuous reflection</p> <p>moderate amplitude related to channel</p> <p>peak frequency : 25 Hz</p> <p>channel width 100-150 m</p> <p>fluvial feature : anastomosing channel and cross-cutting channels</p>
SF8					<p>low to moderate amplitude, continuous reflection</p> <p>peak frequency : 22 Hz</p> <p>fluvial feature : flood plain?</p>

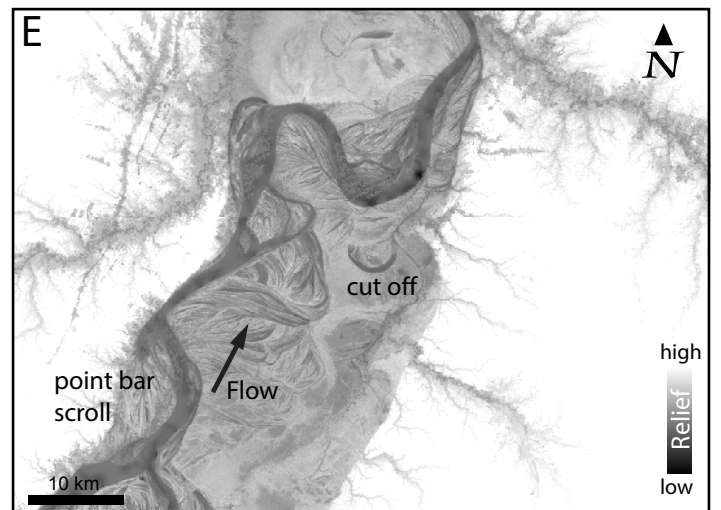
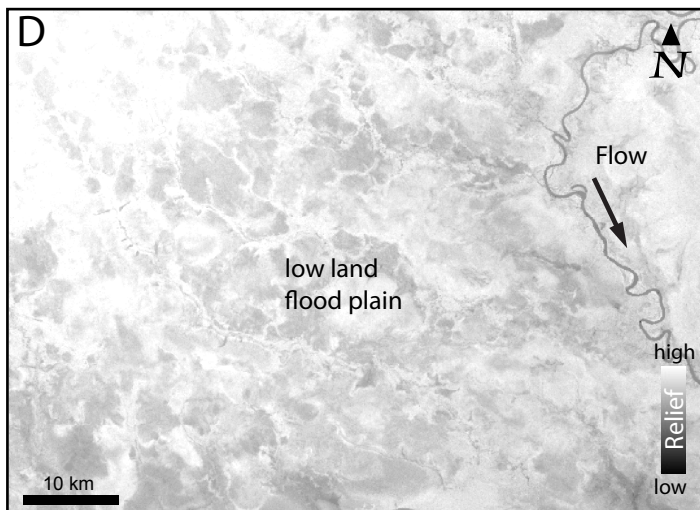
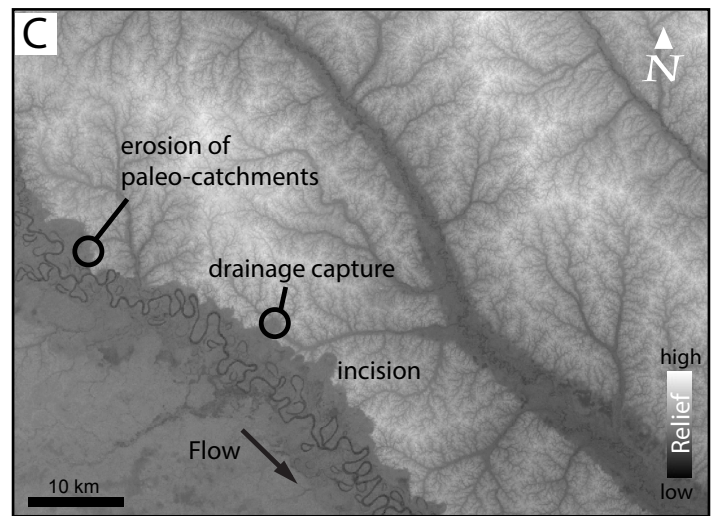
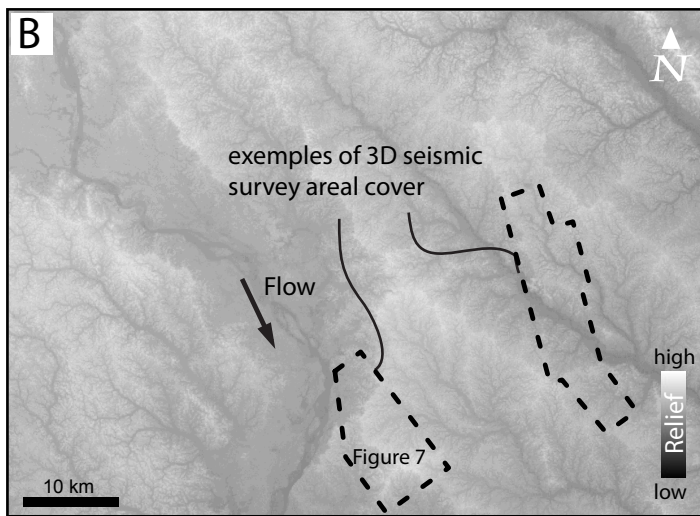
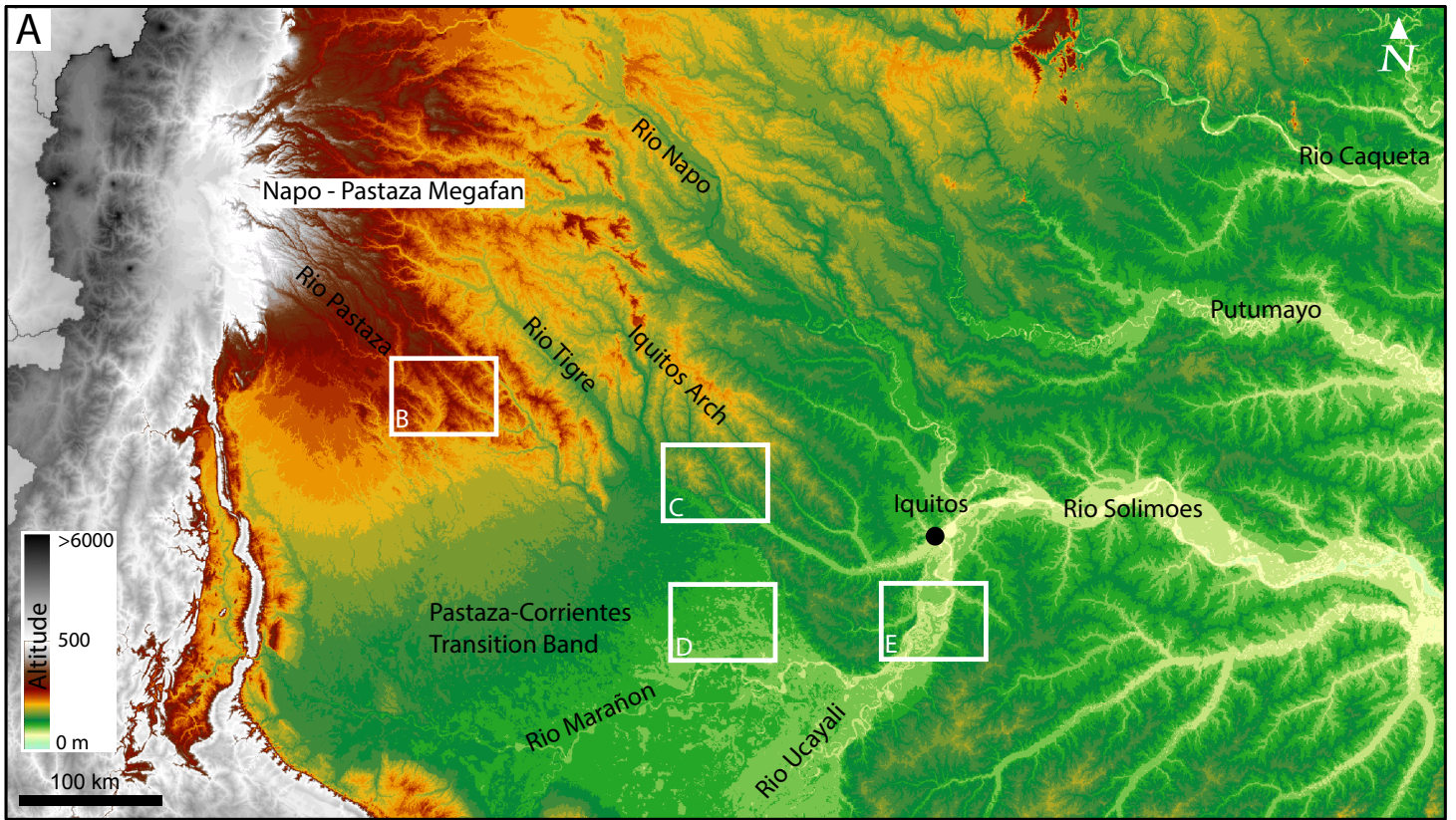




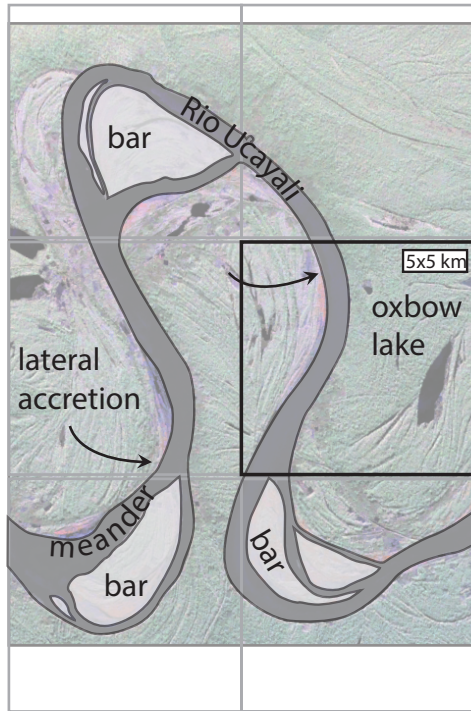




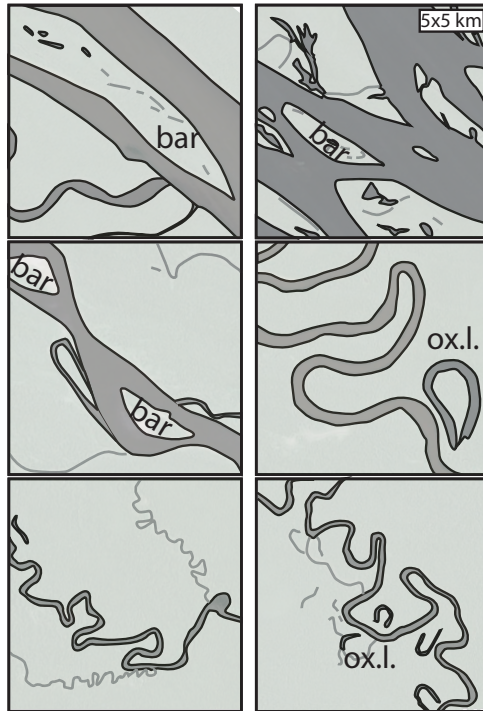




A. UAVSAR



B. Landsat



C. 3D seismic

